DNA damage independent inhibition of NF-κB transcription by anthracyclines

Angelo Chora[1], Dora Pedroso[2], Nadja Pejanovic[1], Eleni Kyriakou[3,4], Henrique Colaço[2], Raffaella Gozzelino[5], André Barros[2], Katharina Willmann[2], Tiago Velho[2,6], Catarina F. Moita[2], Isa Santos[2,7], Pedro Pereira[1], Sílvia Carvalho[1], Filipa Martins[1], João A. Ferreira[1], Sérgio Fernandes de Almeida[1], Vladimir Benes[8], Josef Anrather[9], Miguel P. Soares[10], Arie Geerlof[3,4], Jacques Neefjes[11], Michael Sattler[3,4], Ana C. Messias[3,4], Ana Neves-Costa[2,*] and Luís Ferreira Moita[2,12,*].

[1]Instituto de Medicina Molecular, Faculdade de Medicina, Universidade de Lisboa, 1649-028 Lisboa, Portugal.

[2]Innate Immunity and Inflammation Laboratory, Instituto Gulbenkian de Ciência, Rua da Quinta Grande 6, 2780-156 Oeiras, Portugal.

[3]Institute of Structural Biology, Helmholtz Zentrum München, Ingolstädter Landstr. 1, 85764 Neuherberg, Germany.

[4] Biomolecular NMR and Center for Integrated Protein Science Munich at Department Chemistry, Technical University Munich, Lichtenbergstr. 4, 85747 Garching, Germany.

[5]Chronic Diseases Research Center (CEDOC), NOVA Medical School (NMS), Lisbon, Portugal

[6]Centro Hospitalar Lisboa Norte - Hospital de Santa Maria, EPE, Avenida Professor Egas Moniz, 1649-035, Lisbon, Portugal.

[7]Serviço de Cirurgia, Centro Hospitalar de Setúbal, Setúbal, Portugal

[8]EMBL Genomics Core Facilities, D-69117 Heidelberg, Germany

[9]Feil Family Brain and Mind Research Institute, Weill Cornell Medicine, 407 East 61st Street RR409, New York, NY, 10065, USA.

[10]Inflammation Laboratory, Instituto Gulbenkian de Ciência, Rua da Quinta Grande 6, 2780-156 Oeiras, Portugal.

[11]Department of Chemical Immunology and Oncode Institue, LUMC, Leiden, The Netherlands.

[12]Instituto de Histologia e Biologia do Desenvolvimento, Faculdade de Medicina da Universidade de Lisboa, 1649-028 Lisboa

[*]Correspondence: Ana Neves-Costa, arcosta@igc.gulbenkian.pt and Luis F. Moita, lmoita@igc.gulbenkian.pt

Keywords

Anthracyclines; nuclear factor kappa B (NF-κB); inflammation; DNA damage.

Abstract

Transcriptional programs leading to induction of a large number of genes can be rapidly initiated by the activation of only few selected transcription factors. Upon stimulation of macrophages with microbial-associated molecular patterns (MAMPs), the activation of the nuclear factor kappa B (NF-κB) family of transcription factors triggers inflammatory responses that, left uncontrolled, can lead to excessive inflammation with life-threatening consequences for the host. Here we identify and characterize a novel effect of Anthracyclines, a class of drugs currently used as potent anticancer drugs, in the regulation of NF-κB transcriptional activity in BMDMs, in addition to the previously reported DNA damage and histone eviction. Anthracyclines, including Doxorubicin, Daunorubicin and Epirubicin, disturb the complexes formed between the NF-κB subunit RelA and its DNA binding sites, to limit NF-κB-dependent gene transcription during inflammatory responses, including of pivotal pro-inflammatory mediators such as TNF. We observed that suppression of inflammation can also be mediated by Aclarubicin, Doxorubicinone and the newly developed Dimethyl-doxorubicin, which share anticancer properties with the other Anthracyclines, but do not induce DNA damage in the tested concentrations. This novel mechanism of action of Anthracyclines, contributing to the reduction of inflammation, is thus independent of the activation of DNA damage responses and may be relevant for the development of novel strategies targeting immune-mediated inflammatory diseases.

Introduction

Inflammation plays a critical role in host defense and the maintenance of homeostasis. Microbial-associated molecular patterns (MAMPs) and non-microbial molecules recognition by specialized sensors is a key first step for the initiation of inflammatory responses. These include germline-encoded pattern recognition receptors (PRRs), whose engagement triggers signal transduction pathways leading to the activation of transcription factors that act in a concerted manner to regulate the expression of a large number of genes associated with inflammation [1].

The nuclear factor kappa B (NF-κB) family of transcription factors, comprising RelA, RelB, c-Rel, p100 and p105, plays a prominent role in regulating inflammation [2]. All members share the N-terminal REL-homology domain (RHD) responsible for IκB binding, nuclear localization, dimerization and DNA binding. On their C-terminal region, RelA, RelB and c-Rel contain a transactivation domain (TAD), responsible for their transcriptional activity [3]. While NF-κB activation is strictly required to trigger the inflammatory response, uncontrolled NF-κB activity can result in a failure to resolve inflammation, contributing to the establishment of a growing number of pathological conditions [4].

At steady state, transcriptionally active NF-κB family members, of which RelA is the most abundant, are retained in the cytoplasm by their interaction with inhibitors of κB (IκB) molecules. IκBα phosphorylation in response to a variety of stimuli leads to its proteosomal degradation, a step required for RelA nuclear localization, DNA binding and initiation of gene transcription [5 3]. RelA-dependent IκBα re-synthesis is essential for its nuclear eviction and the timely termination of NF-κB transcriptional activity [6 7]. Posttranslational modifications within both RHD and TAD add an additional layer of control over RelA-dependent gene transcription, activating or repressing its transcriptional activity by controlling RelA association with IκB, nuclear localization, interaction with transcriptional cofactors, DNA binding and stability [8 3].

Anthracyclines have been used as potent anticancer drugs for many decades and doxorubicin (Doxo), in particular, is used in therapies against a wide variety of cancers (reviewed in [9]). Anthracyclines cytotoxicity is mostly derived from their ability to target and inhibit topoisomerase II (TopoII) [10]. In rapidly replicating cells, anthracyclines stabilize the TopoII-DNA cleavable complex therefore potentiating DNA double-strand breaks, the activation of DNA damage responses (DDRs), and ultimately senescence or apoptosis [11 12]. Besides TopoII inhibition, there are a series of other known biological activities of anthracyclines, including DNA intercalation, helicase inhibition and free radical formation, that have been described but their clinical relevance is still poorly understood [9]. More recently, anthracyclines were shown to induce histone eviction from discrete chromosomal regions, which proved to contribute to apoptosis in a TopoII-

independent manner [13] [14]. Cytotoxicity mediated by histone eviction was observed in AML blasts, highlighting the potential clinical impact of these other less exploited activities of anthracyclines [13].

We have previously shown that anthracyclines strongly downregulate cytokine secretion by immune responsive cells challenged with pro-inflammatory stimuli and in mouse models of sepsis [15], a finding recently corroborated in human primary macrophages [16]. In such models, low-dose anthracyclines induce disease tolerance leading to protection against severe sepsis independently of the pathogen load [15]. Whereas the DDR and the DNA damage sensor ATM (ataxia telangiectasia mutated), in particular, are required for anthracycline-mediated induction of disease tolerance, leading to survival to severe infection, the mechanism whereby anthracyclines regulate cytokine production remains obscure [17]. In addition, Epirubicin (Epi) is known to induce the expression and activate ATM in breast cancer cells [18]. Although the role of ATM in DDR has been more extensively documented (signaling orchestrated by ATM is comprehensively reviewed in [19]), ATM is involved in a complex network of signaling pathways including activation of NF-κB [20] [21] [8] [22]. Here we investigate and demonstrate that anthracyclines modulate the inflammatory response in primary macrophages by regulating NF-κB transcriptional activity, independently of the DDR, in a manner that resolves inflammation.

Results

Cytokine secretion and DNA damage

To investigate the role of the DDR in cytokine downregulation mediated by anthracyclines, we used bone marrow-derived mouse macrophages that were activated upon challenge with pro-inflammatory stimuli and tested whether cytokine modulation by Epi requires DNA damage responses (DDR), in particular ATM activation. We began by pre-treating macrophages with Epi and observed that downregulation of cytokine production following *E. coli* challenge was independent of ATM, as Epi led to a dose-dependent decrease in cytokine production not only in WT macrophages, similarly to what was previously reported in the monocytic cell line THP-1 [15], but also in *ATM*$^{-/-}$ macrophages (Fig. 1A). We also tested cytokine secretion in the presence of the ATM inhibitor Ku-55933 and further confirmed that ATM is dispensable for TNF and IL12

downregulation by Epi (Fig. 1B). In agreement with these results, macrophages from WT and from *ATM*$^{-/-}$ animals secreted comparable amounts of the pro-inflammatory cytokines TNF, IL12, IL6 and CXCL10 following activation with fixed *E. coli* (supplementary Fig. 1A). In addition, we confirmed that the doses of Epi used did not induce significant cell death nor did it activate cytokine secretion in the absence of pro-inflammatory stimuli (supplementary Figs. 1B and 1C).

As the regulation of cytokines by Epi did not require ATM activation, we hypothesized that DDR was not required for pro-inflammatory cytokine modulation by anthracyclines. To further explore the lack of interdependency between DNA damage and cytokine modulation by Epi, we tested if other anthracyclines, causing a range of different types and levels of damage to DNA, can also downregulate cytokine secretion. Using the alkaline comet assay we detected DNA damage regardless of the type of strand breaks and we confirmed that Epi causes DNA damage in a time and dose-dependent manner (supplementary Fig. 1D). The amount of DNA damage generated was quantitatively determined using phosphorylation of histone H2AX at Ser139 (γH2AX) as a surrogate marker of DNA damage. In macrophages, γH2AX levels showed that DNA damage is strongly induced by Epi in the range of concentrations that modulate cytokine production (Fig. 1C) and is comparable to that of Etoposide (Eto), another well-studied TopoII inhibitor known to cause DNA breaks and to induce ATM-mediated DDRs (supplementary Fig. 1E; [23] [24]). γH2AX quantification also indicated that the inflammatory challenge does not induce significant extra DNA damage in the conditions used here (supplementary Fig. 1F).

Anthracyclines, a class of drugs consisting of a common tetracycline ring which may be decorated with one or multiple amino sugars (Fig. 1D), have been shown to have a wide range of activities from not causing DNA breaks to being potent inducers of double strand breaks [13]. We observed that the DNA damaging capacity of anthracyclines was also diverse in macrophages: whereas Epi and the closely related Doxorubicin (Doxo) led to a dose-dependent increase in γH2AX signal, Aclarubicin (Acla) and Doxorubicinone (Doxo-none) did not induce significant DNA damage (Figs. 1C and 1E). The comet assay corroborated that DNA damage caused by Acla is similar to the basal levels of damage detected in untreated cells, in sharp contrast with the highly damaging

effects of Epi and Eto (supplementary Fig. 1G). Acla and Doxo-none were then tested for their ability to regulate cytokines. We observed that downregulation of TNF and IL12 production was a common property of the anthracyclines tested, but the modulation caused by Doxo-none was substantially lower than by Epi, Doxo and Acla (Fig. 1F and compare with 1A). Acla led not only to the most pronounced downregulation of TNF but also of the other pro-inflammatory cytokines tested (supplementary Fig. 2A) without inducing significant cell death at the tested doses (supplementary Fig. 2B). To further uncouple DDRs from cytokine modulation by anthracyclines, we asked if Eto and a variant of Doxo that was made incapable of causing DNA damage (but retains a cytotoxic profile similar to Doxo by the introduction of 2 methyl groups in the sugar ring) could downregulate cytokines. Figures 1G and 1H show that TNF was not downregulated by Eto, but was by Dimethyl-doxorubicin (diMe-Doxo). In line with this observation, none of the other anthracyclines tested regulated cytokine production differently in *ATM*$^{-/-}$ macrophages or in the presence of the ATM inhibitor (supplementary Figs. 2C and 2D). Therefore, structural damage to DNA alone is unlikely to explain the observed effect of anthracyclines on cytokine secretion.

Anthracyclines negatively regulate the transcription of NF-κB targets

To investigate the global effects of anthracyclines on gene transcription and their dependence on DNA damage, we performed RNA sequencing (RNAseq) in macrophages treated with either Epi or Acla and challenged with the pro-inflammatory bacterial TLR4 agonist lipopolysaccharide (LPS, supplementary Fig. 3A). The comparison of mRNA expression of macrophages alone with that of 4 h LPS-treated macrophages showed strong induction of pro-inflammatory gene expression in line with the well-described patterns of gene regulation in response to this TLR4 agonist (Fig. 2A, lane 1). A volcano plot revealed that 455 genes were at least 5 fold upregulated in LPS-treated macrophages compared with macrophages alone, whereas only 75 genes were downregulated with the same magnitude by LPS (supplementary Fig. 3B). At the same time, the transcriptome analysis pointed to specific gene expression signatures by Epi and Acla, partly overlapping but not identical, both in the absence of immune challenge (Fig. 2A, lanes 2 and 3) and in the presence of LPS (Fig. 2A, lanes 4 and 5). As anticipated from the cytokine secretion results, Acla led to stronger repression of pro-inflammatory gene expression than Epi (Fig. 2A, compare lanes 4 and 5). The RNAseq data corroborated our observation that cytokines are repressed transcriptionally by Epi

and Acla and we thoroughly validated those results by quantitative RT-PCR. We observed transcriptional downregulation of the cytokines already shown to depend on Epi and Acla - TNF, IL12, IL6 and Cxcl10 - but the regulation also extended to a broader subset of pro-inflammatory mediators (Fig. 2B). Functional analysis of the RNAseq data by DAVID showed that both Epi and Acla transcriptionally repress sets of genes involved in several aspects of innate immune responses, namely cytokine secretion and TNF signaling, amongst other effector functions of the macrophages (supplementary Table 1). We further extended the analysis using GATHER [25] and focused on the molecular signatures behind the genes mutually downregulated by Epi and Acla. The factors controlling the transcription of such genes were identified as mostly belonging to two families of transcription factors: Interferon Regulatory Factors (IRFs) and NF-κB factors (Fig. 2C). To further assess specificity in transcriptional regulation mediated by Epi and Acla, we compared NF-κB-dependent transcription (Fig. 2B) with IRF-dependent transcription (Fig. 2D). We observed that Epi and Acla repress the NF-κB-dependent pro-inflammatory gene profile, as discussed above, but do not lead to downregulation of the IRF-dependent genes tested. In agreement, IFNβ secretion was not modulated by anthracyclines (supplementary Fig. 3C). These results clearly establish that the effect on the LPS-induced signature by anthracyclines cannot be explained by a general decrease in gene transcription. Instead, the observed expression profiles point to a specific negative effect of Epi and Acla on NF-κB transcription, which is compatible with previous observations that the anthracyclines Doxo and Daunorubicin (Dauno) repress TNF-induced NF-κB transactivation in cancer cells [26] [27].

To substantiate the finding that anthracyclines affect transcription, we tested the possibility that mRNA stability of pro-inflammatory genes was affected by anthracyclines. To this end, we treated macrophages with ActD (a Pol I-II/dose-dependent, transcription inhibitor) 2 h after *E. coli* stimulation in the presence and absence of Epi and measured the rate of TNF mRNA decay. We found that the rate of decay was comparable between non-treated and Epi-exposed BMDMs with similar half-lives (65.39 and 61.34 minutes, respectively, supplementary Fig. 3D). This suggested that the observed effect of anthracyclines on NF-κB-dependent gene expression is not due to effects on mRNA stability but differences in transcription.

Next, we tested NF-κB regulation by anthracyclines using a κB luciferase reporter activated by TNF. In HEK293 cells transiently transfected, Epi, Doxo, Acla and Dauno effectively repressed NF-κB reporter expression to basal unstimulated levels (Fig. 2E and supplementary Fig. 3E). We also tested κB reporter transcriptional activity after transduction of a construct expressing full length RelA and anthracyclines still markedly downregulated reporter activity induced by RelA (Fig. 2F). Before, it was shown that Dauno and Doxo activate NF-κB per se, in the absence of inflammatory stimuli, as measured by binding of NF-κB to DNA in EMSA assays (electrophoresis mobility shift assay, [28] [27]). In our luciferase reporter assay, we also observe a slight increase in luciferase reporter activity induced by anthracyclines without TNF (Fig. 2E); however, the negative regulation by anthracyclines in the presence of the pro-inflammatory stimuli is undoubtedly more pronounced (Figs. 2A, B and E).

The prominent regulation of NF-κB transcriptional activity by anthracyclines following pro-inflammatory stimuli was therefore established both for a series of endogenous targets relevant for the inflammatory response but also for a κB binding site-carrying reporter. These observations prompted us to search for the mechanisms whereby anthracyclines are likely to regulate NF-κB nuclear localization and binding to its targets.

Epirubicin affects NF-κB sub-cellular localization

Nuclear NF-κB localization is required for DNA binding and initiation of gene expression [5]. We investigated whether the down-modulation of NF-κB targets by anthracyclines was due to impaired RelA nuclear translocation. RelA nuclear levels in non-treated BMDMs rapidly increased following *E. coli* challenge and slowly relocated overtime being mostly cytoplasmic 4 h after stimulation (Fig 3A, control panel). This is in sharp contrast with BMDM exposed to Epi where the rapid nuclear translocation of RelA upon *E. coli* challenge is not affected, but surprisingly, despite decreased NF-κB-dependent gene expression, RelA remained nuclear at all time points analyzed (Fig 3A, Epi panel). Proteolytic IκBα degradation and re-synthesis is a central mechanism controlling NF-κB sub-cellular localization [5] [6] [7]. Diminished stimulus-induced IκBα synthesis was reported to augment nuclear localization of RelA, an effect not associated with increased NF-κB transcriptional activity [29]. Analysis of IκBα degradation kinetics

revealed that while in non-treated BMDMs IκBα is initially degraded following *E. coli* stimulation with protein levels restored to initial values at 60 minutes, Epi pre-treatment profoundly diminishes IκBα cellular levels at all time points analyzed (Fig 3B). Similar results were observed upon TNF stimulation (supplementary Fig. 3F), demonstrating that the effect of Epi is not stimulus-dependent.

It has been proposed that Doxo has a role in proteosome activation [30]. To assess whether decreased IκBα levels are due to increased proteosome-dependent degradation, we examined IκBα degradation kinetics upon inhibition of the proteasome pathway. While inhibition of proteasome activity by MG-132 treatment 15 minutes following *E. coli* challenge augmented cellular IκBα levels upon de novo synthesis (Fig 3C, upper panel), it failed to restore IκBα levels in cells pre-exposed to Epi (Fig 3C, lower panel). Concomitantly, both Epi and Acla significantly decreased *E. coli*-driven IκBα mRNA expression (Fig. 2B), suggesting that anthracycline pre-treatment hinders IκBα de novo synthesis. This prevents translocation of NF-κB to the cytoplasm therefore breaking the critical negative feedback loop that maintains the cellular responsiveness to subsequent stimuli. We then asked if RelA, while maintained in the nucleus, interacts differently with its target sequences because of anthracyclines.

Epirubicin decreases NF-κB DNA binding

Anthracycline modulation of NF-κB-dependent pro-inflammatory programs was further investigated by chromatin immunoprecipitation in HEK293 cells. Firstly, we assessed the effect of Epi on NF-κB-dependent gene expression in HEK293 cells to assess if these cells replicate the effects of anthracyclines observed in BMDMs. Similarly to BMDMs, pre-exposure of HEK293 cells to Epi significantly reduced TNF and CXCL10 mRNA expression following stimulation with TNF (supplementary Fig. 4A), an effect not associated with detectable cytotoxicity (supplementary Fig. 4B). Moreover, Epi severely impaired RelA nuclear export (supplementary Fig. 4C) as well as IκBα de novo synthesis (supplementary Fig. 4A), supporting the use of HEK293 cells. ChIP at the promoter of target genes revealed that association of the NF-κB subunit RelA following an inflammatory challenge was weakened by pre-treatment with Epi and Acla, whereas binding of RelA to IFNβ promoter was not affected (Fig. 3D). In addition, the recruitment of RNA PolII to the promoter of target genes, including IκBα, was

compromised by Epi and Acla (Fig. 3E). These results are in line with previous observations that Doxo treatment strongly reduced the association of RelA with DNA *in vivo*, which was suggested to be a consequence of altered post-transcriptional modifications in NF-κB subunits in the presence of Doxo, therefore causing the assembly of a defective complex and compromising its DNA binding [27]. In addition, Doxo is also responsible for the decreased recruitment of at least one other transcription factor, HIF-1α, to its target genes [31].

RelA is a protein transcription factor that contains two main domains, the REL-homology domain (RHD) and the transcriptional activity domain (TAD, supplementary Fig. 4D). The RHD contains further the DNA binding domain (DBD), the dimerization domain (DD) and the nuclear localization sequence (NLS). Much of the diversity of transcriptional response is due to RelA binding to DNA regulatory regions, mediated by the DNA binding domain within the amino-terminal region of the RHD [32]. To assess which RelA domain is targeted by Epi, we used two different chimeric DNA constructs composed of the RelA RHD fused to a TAD derived from the Herpes simplex virus VP16 protein (RelA (2-320)-VP16) or a DNA binding domain derived from the bacterial tetracycline repressor (TET) fused to the RelA TAD (TET-RelA (286-551)) [33]. Similarly to the result obtained with full length RelA (Fig 2F), Epi significantly inhibited the transcriptional activity of RelA (2-320)-VP16, as assessed in HEK293 cells transiently co-transfected with the κB-luciferase reporter (Fig. 3F). However, Epi failed to inhibit the transcriptional activity of TET-RelA (286-551) as well as of TET fused to VP16 (TET-VP16) construct, as assessed using a tetracycline operon luciferase (tet°-luc) reporter (Fig. 3F). Together, these results suggest that Epi specifically decreases RelA transcriptional activity by targeting the RelA RHD. While in agreement with published data that anthracyclines inhibit NF-κB transcriptional activity [26 27], our observation that Epi does not affect the RelA TAD argues against the established mechanism of NF-κB regulation by Doxo and Dauno in cancer cells [26]. Of notice, the effect of anthracyclines on RelA RHD has not been previously assessed. Whereas this apparently distinct mechanism of action of anthracyclines could depend on the cell type as well as the context of NF-κB activation, it also reflects the immense complexity behind NF-κB-regulated transcription, in particular the variety of factors contributing to altered DNA binding, such as the presence of multiple κB binding sites or competition from other

transcription factors [34]. Compelling results obtained with both full length RelA or RelA-RHD have brought to light that *in vitro* DNA-binding affinities of NF-κB subunits insufficiently predict transcriptional outcomes [34].

Epirubicin and aclarubicin disturb RelA-DNA binding

In order to understand how Epi and Acla can affect NF-κB DNA affinity and transcription of its targets, we performed *in vitro* assays in order to characterize the binding of Epi and Acla to DNA, RelA and DNA-RelA complexes. For our *in vitro* studies, we used a 14-mer DNA sequence (5'-CTGGAAATTTCCAG-3') derived from the κB-33 promoter DNA sequence [35]. As expected, the anthracyclines Epi and Acla, bind to the DNA. By NMR spectroscopy, we see significant spectral changes in the imino region of the DNA after the addition of the compound (data not shown), which are consistent with binding. Using ITC, we found that Epi and Acla bind to the DNA duplex with an equilibrium dissociation constant (K_D) of 11.4 μM and 7.3 μM, respectively (Table 1). Acla binds slightly stronger to DNA than Epi. In the literature, the affinity of Acla to different DNA molecules has been reported to be in the low nM to low μM range [36–38], whilst compounds similar to Epi, like Doxo, that differs from Epi in the stereochemistry of the 4'-OH group, binds to DNA in the nM range [39]. It is known that most of the anthracyclines have a preference for GC-rich sequences. More specifically, the aglycon chromophore of the anthracycline intercalates at a pyrimidine–purine step, while the sugar part interacts with the DNA minor groove [40–42]. Indeed, it has been shown that Epi has a preference for GC-rich sequences, with crystal structures showing that epirubicin stacks between 5'-CG-3' or 5'-TG-3', suggesting that YG sequences are preferred by Epi. In the κB-33 DNA oligonucleotide, there are two 5'-TG-3' motifs, indicating that up to two molecules of Epi can bind to it.

A crystal structure of RelA RHD in complex with the κB-33 promoter DNA target (5'-CGGCTGGAAATTTCCAGCCG-3') has revealed that DNA mainly contacts the interface between the dimerization and the DBD domains (supplementary Fig. 5A). In this structure, one of the protein subunits recognizes a 5'-GGAA-3' half site, while the other one recognizes a 5'-GAAA-3' (supplementary Fig. 5A)[35]. We used a 14-mer DNA sequence (5'-CTGGAAATTTCCAG-3') derived from the κB-33 promoter DNA sequence to test binding to a construct of RelA RHD (residues 19-291) containing DBD and DD domains. Titration of DNA to RelA revealed that the DNA binds strongly to the protein with an affinity of 690nM by ITC for the RelA-κB-33 interaction (supplementary

Fig. 5B and Table 1). The affinity of our DNA sequence is slightly different from the reported value of 256nM [43], likely reflecting the difference in the sequence length (14-mer versus 18-mer), the construct origin and the method used. Notably, the DNA-protein interaction is endothermic, i.e. enthalpically unfavorable and thus entropy-driven. Using static light scattering (SLS) experiments we could confirm that both the protein and the DNA form dimers (data not shown). However, the protein-DNA complex was not observed, due to a very fast off-rate [44].

We used NMR spectroscopy to study the effect of the small molecules Epi and Acla on RelA-DNA binding. Double titration experiments were performed in two ways: (1) RelA was initially titrated with the anthracycline and then with DNA; (2) RelA was first titrated with DNA and then with compound. The results showed that, in the presence of anthracyclines, RelA is still able to bind the promoter DNA. However, the final spectra differ (Fig. 4A), suggesting that the anthracyclines affect the RelA-DNA complex differentially. Residues particularly affected by Epi are R50, K56, K62, T78, K79, H88, E89, Q119, A129 and V157 in the DBD domain and A192, H245, I250 and V268 in the DD domain. Addition of Acla to RelA-DNA complexes causes precipitation of the protein and therefore it is more difficult to follow changes, but residues H88, Q119, A129 and N186 from DBD and H245 from the DD domain are affected. Remarkably, though Epi binds with slightly lower affinity and lower stoichiometry to the DNA than Acla, it seems to more strongly disturb the RelA-DNA complex (Fig. 4A and Table 1). This is attested by the fact that the addition of Epi to the RelA-DNA complex causes NMR chemical shift changes for some backbone amide signals in RelA towards an unbound state (Fig. 4B left), an effect that is not observed upon Acla addition (Fig. 4B right). The residues that are affected by the addition of either compound are distributed in both DBD and DD and largely coincide with the DNA binding region for both compounds. Differences in binding surface likely reflect the different chemical moieties present in the two compounds. Specifically, Acla contains three sugar rings instead of one in case of Epi. We have shown that the compounds bind to the protein through their sugar parts, but there are crystal structures showing that anthracyclines sugar moiety binds to the minor groove of the DNA. A number of studies have shown the important role of the amino group at the 3′ position of the sugar moiety for drug DNA binding affinity and antitumor activity [40,45]. Our *in vitro* binding results are in agreement with our

biological results, suggesting that that both compounds bind to the DNA sequence, disturbing the RelA-DNA complex.

In order to understand how anthracyclines affect the RelA-DNA complex we performed ITC competition experiments. We observed that the binding affinities upon DNA titration to a pre-formed complex of protein with the compound are similar to the binding affinities for the DNA to the protein alone (Table 1). However, the thermodynamic features of the interaction are different: binding of DNA to RelA is entropy-driven and endothermic, whilst binding of DNA to RelA incubated with anthracyclines is enthalpy-driven and exothermic. Surprisingly, when DNA with a 2-fold excess of Epi is titrated to the protein (Table 1), the binding affinity decreases dramatically from a K_D of 690nM to 5000 nM. This suggests that when anthracyclines-DNA complex is formed, binding to RelA is more affected. We have also tested a potential direct binding of Epi and Acla with the protein. Both compounds bind weakly to the protein as indicated by NMR spectroscopy (supplementary Figs. 6 and 7). In 2D-TROSY NMR protein spectra (supplementary Fig. 7) we did not observe significant backbone amide changes after the addition of the compound, indicating that the compounds bind very weakly to the protein. Binding to the protein, though weak, is mediated through the compound sugar part as observed in STD experiments (supplementary Fig. 6). Importance of the sugar moiety to binding was supported by a control experiment with Doxo-none that lacks the sugar part and does not show any binding to RelA by STD NMR (supplementary Fig. 6C). Binding of anthracyclines to RelA using ITC experiments (Table 1) was not detected as expected, since ITC is not suitable for very weak binding.

Discussion

In closing, we provide evidences that anthracyclines can suppress NF-κB-dependent gene transcription during inflammatory responses, namely of critical pro-inflammatory mediators such as TNF (Figs. 1 and 2). Despite the general notion that anthracyclines induce NF-κB-dependent anti-apoptotic gene expression when used as chemotherapeutic drugs [28] [46] [47], Doxo and Dauno can also repress NF-κB activity probably depending on cell and tumor type [26] [27]. Due to the genotoxicity associated with the classically studied anthracyclines, and in light of our previous observations that Epi is protective in sepsis through ATM-mediated signaling [15], we attempted to dissect if

cytokine regulation by anthracyclines was dependent on the induction of DNA damage responses. We used a selection of anthracyclines that, unlike Epi, do not cause detectable DNA damage in the conditions tested. Whereas pro-inflammatory gene expression orchestrated by NF-κB was still hindered by Acla, Doxo-none and the newly developed diMe-Doxo (Figs. 1F, 1H), we showed that DNA damage is not required for repression of NF-κB (Figs. 1A, 1B and supplementary Figs. 1C, 1D). Instead, the prevailing mechanism is likely to be through anthracycline-mediated modulation of the interaction of NF-κB with its targets (Fig. 3D).

Our biophysical and structural studies further suggest a novel mechanism of action for anthracyclines, independent of DNA damage and induction of ATM. Here we showed that Epi and Acla disturb the complexes formed between the NF-κB subunit RelA and its DNA binding sites (Fig. 4A). Remarkably, Epi is more potent at perturbing the RelA-DNA complexes than Acla, despite the fact that Acla is a stronger down-regulator of NF-κB-dependent gene expression. It will be important to structurally dissect which other effects are responsible for the higher efficiency of Acla in blocking transcription of NF-κB genes. We observed that the residues that are affected by the addition of Epi and Acla are distributed in both the DBD (DNA binding domain) and the DD (dimerization domain) of the RelA RHD (REL-homology domain) and close to the DNA binding region in both cases. These *in vitro* binding results corroborate our reporter assays that revealed that Epi downregulates RelA transcriptional activity by targeting the RHD (Fig 3F). Importantly, the two anthracyclines differ in their structures and more specifically in their sugar part, as Acla contains three sugar rings instead of one in case of Epi. We have shown that the compounds bind to RelA through their sugar parts, which was confirmed by comparing with Doxo-none that lacks the sugar and therefore did not bind to RelA (supplementary Fig. 6). However, there are crystal structures that also show the sugar moiety of anthracyclines binding to the minor groove of the DNA and a number of studies have shown the important role of the amino group at the 3′ position of the sugar moiety for drug DNA binding affinity and antitumor activity. It is possible that, in addition to direct binding to RelA, both Epi and Acla bind to DNA bases within the κB motif, therefore further disturbing the RelA-DNA complex (Table 1). Notably, the engagement of RelA and other NF-κB factors with kB sites has been shown to be highly dynamic and regulated by the genomic context and by other nuclear factors, which are

central aspects expected to play major roles in NF-κB-orchestrated transcriptional programs [34].

To conclude, a better understanding of the underlying molecular mechanisms of anthracycline action may be required for the development of novel strategies for the treatment of immune-mediated inflammatory diseases such as rheumatoid arthritis, asthma and inflammatory bowel disease.

Figure legends

Figure 1 – Anthracyclines regulate cytokine secretion independently of ATM.
A, Cytokine secretion (TNF, IL12, IL6 and Cxcl10) was quantified by ELISA following *E. coli* challenge in the presence of various doses of Epirubicin (Epi) in WT and ATM-/- macrophages; **B**, Cytokine secretion (TNF and IL12) was quantified by ELISA following *E. coli* challenge in macrophages treated with various doses of Epi and the ATM inhibitor KU-55933; **C**, H2AX phosphorylation was quantified by ELISA in macrophages treated with various doses of Epi; **D**, Schematic representation of the molecular structures of the anthracyclines Epi, Aclarubicin (Acla), Doxorubicin (Doxo) and Doxorubicinone (Doxo-none); **E**, H2AX phosphorylation was quantified by ELISA in macrophages treated with Doxo, Acla and Doxo-none; **F**, TNF and IL12 secretions following *E. coli* challenge were quantified by ELISA in macrophages treated with Doxo, Acla and Doxo-none; **G**, **H**, H2AX phosphorylation was quantified by ELISA in macrophages treated with Etoposide (Eto) and Dimethyl-doxorubicin (diMe-Doxo) and TNF secretion following *E. coli* challenge was quantified by ELISA in macrophages treated with Eto and diMe-Doxo. The assays show arithmetic means and standard deviations of technical replicates from one representative animal of at least 3 independent animals tested. Unpaired t test; *P<0.05; **P<0.01; ***P<0.001

Figure 2 – Anthracyclines regulate NF-κB-dependent transcription.
A, RNAseq in macrophages stimulated with LPS for 4h and treated with Epirubicin (Epi) or Aclarubicin (Acla); **B**, Gene expression was quantified by quantitative RT-PCR in macrophages following *E. coli* challenge and treated with various doses of Epi and Acla; **C**, GATHER analysis of Epi and Acla repressed genes in the subset of LPS-upregulated

genes; **D**, Gene expression of IFN genes was quantified by quantitative RT-PCR in macrophages following *E. coli* challenge and treated with various doses of Epi and Acla; **E**, Luciferase quantification of a κB reporter in HEK293 cells stimulated with TNF and treated with 50nM of Epi, Doxorubicin (Doxo) and Acla; **F**, Luciferase quantification of a κB reporter in HEK293 cells treated with 2μM of Epi, Doxo and Acla in the absence or presence of a vector overexpressing RelA. A, B and D show arithmetic means and standard deviations of technical replicates from one representative animal of at least 3 independent animals tested.

Figure 3 – Anthracyclines affect RelA sub-cellular localization.
A, RelA immunolocalization in macrophages challenged with E. coli and left untreated (control) or treated with Epirubicin (Epi) 2μM. **B**, IκBa degradation kinetics in macrophages following *E. coli* challenge in the absence or presence of Epi 2μM for 1h. **C**, Macrophages were either left untreated (top panel) or treated with Epi (bottom panel) and challenged with *E. coli* for the indicated times. **D**, Macrophages were challenged with LPS, treated with Epi or Acla 2μM and an antibody anti RelA was used to immunoprecipitate the associated chromatin, from where the promoter sequences of IκBα, TNF and IFNβ were amplified; **E**, HEK 293 cells were challenged with TNF, treated with Epi or Acla 2μM and an antibody anti PolII was used to immunoprecipitate the associated chromatin, from where the promoter sequence of IκBα was amplified; **F**, HEK 293 cells were transiently transfected with the κB-luc reporter alone or in conjunction with full length RelA or RelA (2-320)-VP16 or TET-RelA (268-551) and cells were left untreated or treated with Epi 2μM for 16h.

Figure 4 – Epirubicin and Aclarubicin disturb RelA-DNA binding.
A, Superposition of 2D $^{1}H,^{15}N$ NMR correlation spectra of 100μM $RelA_{19-291}$ free protein (black), in the presence of 100μM κB-33 DNA (red) and upon additional presence of 500 μM Epi (green, left) or 500μM Acla (green, right). All spectra were recorded at 800MHz, 20 °C, 16 scans. **B**, Crystal structure of RelA REL-homology domain (RHD), containing the DNA binding domain (DBD, light blue residues) and the dimerization domain (DD, yellow residues), in complex with κB-33 promoter DNA target (olive green and pink) and the effect of adding Epi (left) and Acla (right); the

DNA binding residues are depicted in red, whereas the residues that shift after addition of the anthracyclines are depicted in blue.

Table 1 – Summary of the data obtained by Isothermal Titration Calorimetry (ITC) competition experiments to determine the effect of Epirubicin and Aclarubicin on RelA-DNA binding.

Supplementary Figure 1 – Control experiments for cytokine regulation by Epirubicin and characterization of DNA damage by Epirubicin.

A, In the absence of challenge, WT and ATM-/- macrophages secrete similar amounts of the cytokines TNF, IL12, IL6 and Cxcl10, as observed by ELISA; **B**, Cell number quantification using Alamar Blue fluorescence in unstimulated macrophages or macrophages stimulated with *E. coli*, both treated with various doses of Epirubicin (Epi); **C**, Cytokine secretion quantified by ELISA (TNF, IL12, IL6 and Cxcl10) is only detected in cells stimulated with *E. coli* and is not detected in unstimulated cells left untreated or treated with 2µM of Epi; **D**, Percentage of broken DNA in the comet tail as quantified by Comet assay in THP-1 cells treated for 15, 30, 60 and 120 min with Epi or Etoposide (Eto); **E**, H2AX phosphorylation was quantified by ELISA in macrophages treated with various doses of Epi and Eto; **F**, Similar to F but the macrophages were either stimulated with *E. coli* for 4h our left unstimulated; **G**, Similar to D but the treatments were for 120 min with Aclarubicin (Acla) and Eto 1µM. The assays show arithmetic means and standard deviations of technical replicates from one representative animal of at least 3 independent animals tested. Unpaired t test; *P<0.05; **P<0.01; ***P<0.001

Supplementary Figure 2 – Similarly to Epirubicin, Aclarubicin regulates cytokine secretion independently of ATM.

A, Cytokine secretion (TNF, IL12, IL6 and Cxcl10) in macrophages was quantified by ELISA following *E. coli* challenge in the presence of various doses of Aclarubicin (Acla); **B**, Cell number quantification using Alamar Blue fluorescence in unstimulated macrophages treated with various doses of Acla; **C**, TNF and IL12 secretion was quantified by ELISA following *E. coli* challenge in the presence of various doses of Acla in WT and ATM-/- macrophages; **D**, TNF and IL12 secretion was quantified by ELISA following *E. coli* challenge in macrophages treated with various doses of Acla and the

ATM inhibitor KU-55933. The assays show arithmetic means and standard deviations of technical replicates from one representative animal of at least 3 independent animals tested.

Supplementary Table 1 – Functional analysis of Epirubicin and Aclarubicin repressed genes.

DAVID functional analysis of the RNAseq data in macrophages stimulated with LPS for 4h; the table shows representative clusters of genes downregulated by Epirubicin (Epi) or Aclarubicin (Acla).

Supplementary Figure 3 – Testing specificity of transcriptional regulation by anthracyclines.

A, RNAseq analysis workflow; **B**, Interferon beta secretion was quantified by ELISA following *E. coli* challenge in macrophages treated with various doses of Epirubicin (Epi, left) and Aclarubicin (Acla, right); One assay representative of 2 independent experiments. **C**, Analysis of TNF mRNA stability in macrophages treated with Epi 2□M for 1h or untreated; Actinomycin D was added 2h after *E. coli* stimulation; **D**, Luciferase quantification of a κB reporter in HEK293 cells treated with 2μM of Daunorubicin (Dauno) in the absence or presence of a vector overexpressing RelA; **E**, IkBα degradation kinetics in macrophages following TNF challenge in the absence or presence of Epi 2μM for 1h.

Supplementary Figure 4 - Epirubicin modulates NF-κB activity in HEK-293 cells.

A, TNF, Cxcl10 and IKBA mRNA levels in HEK 293 cells challenged with TNF for 4 hours and treated with Epirubicin (Epi); **B**, HEK 293 cells were left untreated (control) or exposed to Epi for 16 hours. Cell viability was evaluated by flow cytometry based on Live/Dead and Annexin V staining. One representative of 2 independent assays; **C**, RelA immunolocalization in HEK 293 cells left untreated (control) or exposed to Epi 5μM for 1 hour, at indicated time points, followed by TNF challenge. One assay representative of 3 independent experiments; **D**, Schematic representation of RelA sequence with functional domains.

Supplementary Figure 5 –RelA RHD binding to κB-33 promoter DNA

A, 3D structure of RelA RHD in complex with κB-33 promoter DNA (PDB 1RAM). The DD domain and DBD are shown in yellow and cyan, respectively. In dark red are represented the residues that interact with the DNA. The DNA is shown in green with nucleotides contacting the protein colored orange. B, NMR binding studies on RelA RHD domain with a 14-mer DNA sequence (5'-CTGGAAATTTCCAG-3') derived from the κB-33 promoter DNA. 2D $^{1}H,^{15}N$ correlation spectra of 100 μM $RelA_{19-291}$ recorded without (black) and with 100 μM DNA (red) (800 MHz, 20 ºC, 16 scans).

Supplementary Figure 6 –STD NMR experiments to test the interaction of RelA with A, Epirubicin, B, Aclarubicin and C, Doxorubicinone. The blue spectra correspond to the reference buffer. The green spectra are recorded with 500μM of each compound in d11-Tris-HCl pH 7.5, 75mM NaCl and 10% D_2O buffer (600MHz, 20ºC, 128 scans). Red spectra correspond to the 1D spectra of the compounds with protein in buffer. The black spectrum shows STD signals for each compound. On the right side of each set of spectra, a zoomed view is shown. In all STD experiments, the arrow indicates the irradiation region (0.05ppm) (600MHz, 20ºC, 800 scans).

Supplementary Figure 7 – NMR binding studies on $RelA_{19-291}$ with Epirubicin (Epi) and Aclarubicin (Acla). Superposition of 2D $^{1}H,^{15}N$ NMR correlation spectra of 100μM $RelA_{19-291}$ recorded without (black) and with a) 500μM Epi (red) or b) 500μM Acla (red) (800MHz, 20ºC, 16 scans).

Supplementary Figure 8 – Comparison of the order of addition in NMR competition binding studies of epirubicin and aclarubicin. Superposition of 2D $^{1}H,^{15}N$ correlation spectra of 100μM $RelA_{19-291}$ with 100μM DNA (black) with (left) 100μM $RelA_{19-291}$ with 100μM DNA and 100μM epirubicin (red) and 100μM $RelA_{19-291}$ with 500μM epirubicin and 100μM DNA (green), and with (right) 100μM $RelA_{19-291}$ with 100μM DNA and 500μM aclarubicin (red) and 100μM $RelA_{19-291}$ with 500μM aclarubicin and 100μM DNA (green) (800MHz, 20ºC, 16 scans).

Methods

Reagents. Epirubicin, doxorubicin, daunorubicin, doxorubicinone and dimethyl-doxorubicin were dissolved in PBS at 1mg/mL, stored at -80ºC and used at the indicated final concentrations. Anthracyclines were from various commercial sources except for

dimethyl-doxorubicin, which was a gift from Jacques Neefjes. Etoposide (Sigma Aldrich) was dissolved in DMSO and used at indicated final concentrations. MG132 was dissolved in DMSO and used at a final concentration of 10µM. ATM inhibitor KU-55933 (Sigma Aldrich) was dissolved in DMSO and used at a final concentration of 5µM. Human recombinant TNF (PeproTech) was dissolved in RPMI and used at a final concentration of 10ng/mL for the indicated times. Actinomycin D (ActD) (AppliChem) was dissolved in DMSO and used at a final concentration of 5µg/mL for the indicated times. LPS (from *E. coli* K12, Invivogen) was dissolved in RPMI and used at a final concentration of 100ng/mL. PFA-fixed *E. coli* was prepared as before [48] in house and added to the medium at a ratio of 20 bacteria per cell. AlamarBlue cell viability assay (Invitrogen) was used to determine cell viability according to the manufacturer's instructions.

Generation of bone marrow-derived macrophages and cell culture. Total bone marrow cells were flushed from femurs and tibiae, counted and seeded ($3x10^6$ cells/mL) in RPMI 1640 supplemented with 10% (v/v) FBS, 0.2% (v/v) Penicillin-Streptomycin, 1% (v/v) Pyruvate, 1% (v/v) L-Glutamine, 1% (v/v) non-essential aminoacids, 1% (v/v) Hepes buffer and 0.05 M of 2-Mercaptoethanol (all Gibco) supplemented with 30% conditioned medium from mouse macrophage colony stimulating factor (M-CSF)-producing L929 cells. On day 7, adherent BMDM cells were collected, counted, reseeded in 96-well plates (5×10^4/well) and treated and/or challenged as indicated. HEK293 cells were obtained from ATCC and cultured in DMEM supplemented with 10% (v/v) FBS, 1% (v/v) Penicillin-Streptomycin and 1% (v/v) non-essential aminoacids (all Gibco). Cells were cultured in a humidified atmosphere containing 5% CO_2.

Cytokine production measurement. Cell culture supernatants were collected at indicated time points and TNF, Cxcl10, IL6, IL-12p40 and IFNβ production quantified using ELISA MAX Standard kits (Biolegend) according to the manufacturer's instructions.

qRT-PCR. Total RNA was isolated from BMDM using the RNeasy Mini Kit (Qiagen), reverse transcribed with superscript II reverse transcriptase (Invitrogen) and specific RNA specimens were quantified by PCR reaction using SYBRgreen Supermix (Bio-Rad) on the QuantStudio7 Flex real-time PCR system (Applied Biosystems). Cycle thresholds (Ct), normalized to Ct of GAPDH, were used to calculate fold increase over control. Primer sequences are described in the supplementary information section.

RNA-seq and data analysis. Total RNA was extracted as described above and quality was assessed using the AATI Fragment Analyzer. Samples with RNA Quality Number (RQN) >8 and clearly defined 28S and 18S peaks were further used for preparation of mRNA libraries, which were pooled and sequenced (75 bp, single end) using NextSeq500. The quality of the sequences was assessed using FASTQC and MultiQC before the alignment [49]. Sequences were aligned against the *Mus musculus* genome version 89, with the annotation file for the genome version 89, both from Ensembl. The alignment was done with STAR [50], using the default parameters and including the GeneCounts option. The files from GeneCounts were imported to R (version 3.5.1), taking into account the strandness associated with the sequencing protocol. DESeq2 (version 1.22.1) [51] was used for the downstream analysis. Heatmaps were created with data normalized from raw counts through Regularized Log Transformation (rlog) [51]. The log2FC was shrunk using the 'ashr' (Adaptive SHrinkage) package [52] and genes were considered differentially expressed when the p-value was below 0.05 after adjusting using false discovery rate (FDR). Gene Information was obtained from org.Mm.eg.db.

Antibodies used in Western Blot and Immunofluorescence. The following antibodies were used for the specific detection of: IκBα, sc-371, Santa Cruz; RelA, sc-372, Santa Cruz; RelApS536, 3031, Cell Signaling; and β-actin, sc-58673, Santa Cruz. Primary antibodies were detected using HRP-conjugated secondary antibodies (Cell Signaling).

Transient transfection and Reporter assay. N-terminal Myc-tagged RelA, RelA (2–320)/VP16, TET/RelA (268–551) and TET/VP16 expression vectors, the NF-κ firefly luciferase reporter construct (*κB-luc*), the tetracycline operon (tet°) firefly luciferase reporter (*tet°-luc*), were previously described [33]. The pSV-β-galactosidase reporter (Promega) consists of the lacZ gene from *E. coli* under the control of the SV40 early promoter and enhancer, providing for constitutive expression in cells. Transient transfections were carried out using the calcium phosphate precipitation method. 24 hours after transfection, cells were either pre-exposed to epirubicin for 1 hour prior to TNF stimulation or treated with epirubicin for 16 hours in the RelA over-expression assays. After incubation, cells were lysed with passive lysis buffer (Promega) and firefly luciferase and β-galactosidase activity were measured using the Luciferase Assay System (Promega) and Galacto-Ligh System (Applied Biosystems), respectively, following the manufacturer's instructions.

Chromatin Immunoprecipitation (ChIP). Chromatin immunoprecipitation (ChIP) was performed on HEK293 cells as previously described [53]. Antibodies against RelA (sc-372, Santa Cruz) and RNAPII (sc-899, Santa Cruz) were used for immunoprecipitation.

Comet assay. Comet assay was performed in THP-1 cells (ATCC catalog number TIB-202) using the CometAssay Kit 25 x 2 well slides (Trevigen catalog number 4250-050-K). A step-by-step protocol detailing the exact procedures and all the materials used is available online from Protocol Exchange (Alkaline Comet Assay using the monocytic cell line THP-1, https://doi.org/10.21203/rs.2.11936/v2).

phosphoH2AX quantification. Phosphorylation of histone H2AX at serine 139 was quantified by cell-based ELISA using the kit Human/Mouse/Rat Phospho-Histone H2AX (R&D catalog number KCB2288), according to the manufacturer's instructions.

Purification of recombinant RHD RelA. A human RelA construct (residues 19-291) was prepared by subcloning into pETM11 vector, which contains an N-terminal His6-tag and a TEV protease cleavage site. The new construct contains the N-terminal DNA-binding domain (DBD, residues 19-191) and the C-terminal dimerization domain (DD residues 192-291). The plasmids were transformed into *E. coli* strain BL21 (DE3) cells and cultured overnight at 20°C in LB media supplemented with 100µg/ml kanamycin (SERVA Electrophoresis GmbH).

For the preparation of uniformly ^{2}H (~100%), ^{15}N (99%)-labeled protein was expressed at 37°C using M9 minimal medium containing $^{15}NH_4Cl$, [^{12}C]D-d7-glucose(2g/L) (97% D, Sigma-Aldrich) in 100% D_2O. A standard protocol of sequential pre-cultures for better D_2O adaptation over a 3d period was followed to increase the yield of protein expression in 100% D_2O. On the first day, a 25 ml preculture in LB medium was prepared and grown overnight at 37°C. Next day, a preculture of 50 ml M9 minimal medium in H_2O was inoculated with 1 ml of the overnight LB preculture and grown at 37°C. After some hours, when the preculture reached an optical density at 600nm (OD600) close to 0.6 was spun down for 10min at 3,202 *g*. The cells were resuspended in 1ml of M9 medium in 100% D_2O and used for the inoculation of 100ml of M9 medium in 100% D_2O, such that the OD600 was 0.1-0.15. This small culture was left overnight at 37°C. The next day, this culture was added to 900ml of M9 medium in 100% D_2O. All cultures in minimal media were induced at 0.8 OD600 with 0.5mM of IPTG overnight at 20°C.

After overnight induction, cell pellets were lysed by sonication in lysis buffer (50 mM Tris-HCl pH 8, 300 mM NaCl, 5 mM imidazole, 5 mM mercaptoethanol, 0.025 mg/ml DNAse I, 0.1 mg/ml Lysozyme (SERVA Electrophoresis), 2.5 mM $MgSO_4$, 0.1% NP-40 (Nonidet P40, Applichem) and 1 pill of protease inhibitor EDTA-free (cOmplete Tablets, Mini EDTA free, Roche diagnostics) per 30 mL lysate. The cell lysate was centrifuged at 60,000 *g* for 30 min at 4 °C. After filtration, the His-tagged protein in the supernatant was loaded on an IMAC (Immobilized Metal Affinity Chromatography). The supernatant was applied to Ni-NTA resin (QIAGEN) previously equilibrated with 3 column volumes of buffer A (50 mM Tris-HCl pH 8, 300 mM NaCl, 5 mM imidazole, 5 mM mercaptoethanol). Bound protein was washed with 3 column volumes of buffer A and unspecific bound protein was washed away with 3 column volumes of Wash Buffer (50 mM Tris-HCl pH 8, 1 M NaCl, 5 mM Imidazole and 5 mM mercaptoethanol). His_6-tagged protein was eluted using elution buffer (50 mM Tris-HCl pH 8, 300 mM NaCl, 300 mM Imidazole and 5mM mercaptoethanol). The affinity His-tag was removed from the protein by TEV (1:5 protein:TEV ratio) cleavage during dialysis into 50 mM Tris-HCl pH 8, 300 mM NaCl and 5 mM mercaptoethanol buffer overnight at 4 °C. The cleaved tag and TEV protease were removed from the target protein using a second IMAC step in dialysis buffer. The fractions containing RelA were pooled, concentrated and further purified by size-exclusion chromatography (SEC) using a Superdex 75 Hiload 16/60 column (S75, GE Healthcare). The SEC buffer used was 50 mM Tris-HCl pH 7.5, 150 mM NaCl, 1 mM EDTA and 5mM Dithiothreitol (DTT). For the ^{2}H, ^{15}N-labeled RelA, prior to the SEC purification step, 2M urea were added to the protein sample for 1 hour, in order to enhance the proton chemical exchange. The final yields were 12.5 mg for ^{2}H, ^{15}N RelA and 52 mg for unlabeled RelA per liter of cell culture.

For NMR experiments, all protein samples were exchanged by successive concentration/dilution steps into NMR buffer (100mM d11-Tris-HCl (Cortecnet) pH 7.5, 75mM NaCl, and 5mM d10-DTT (Cortecnet), 90% H_2O/10% D_2O). The protein concentrations were calculated using the absorption at 280nm wavelength with a Nanodrop 2000 (Thermo Fisher Scientific), by using molar extinction coefficients of 17420 M^{-1} cm^{-1} for $RelA_{19\text{-}291}$.

NMR Spectroscopy. One-dimensional (1D) ^{1}H NMR experiments were recorded using a WATERGATE pulse sequence at 25°C on a Bruker AvanceIII 800MHz spectrometer equipped with a cryogenic TCI-probehead (^{1}H, ^{31}P, ^{13}C, ^{15}N) equipped with Z-gradients.

1D ^{1}H experiments were performed using a WATERGATE pulse sequence with 32k time domain and 128 scans in 100mM d11-Tris-HCl pH 7.5, 75mM NaCl, 5mM d10-DTT and 10% D_2O. STD experiments were recorded using an interleaved pulse program with on-resonance protein irradiation at 0.15ppm for epirubicin, 0.5ppm for aclarubicin and 0.6ppm for doxorubicinone and off-resonance irradiation at -5ppm with 2sec effective irradiation, using 800 scans and 32k time domain points (600MHz). Each experiment was performed using 500µM of compound and 10µM of unlabeled protein. Reference STD experiments without protein were performed at the same conditions, using the same irradiation regions. Spectra were processed using TOPSPIN 3.2 (Bruker Biospin, Rheinstetten, Germany).

NMR binding studies were performed at 25°C using 100µM ^{2}H(~100%), ^{15}N-labeled $RelA_{19\text{-}291}$ dimer in a 100mM deuterated d11-Tris-HCl buffer (pH 7.5, 75mM NaCl, 5mM d10-DTT and 10% D_2O) by adding compound to a final concentration of 500 and/or 100µM of duplex-DNA, and monitoring the changes by ^{1}H, ^{15}N TROSY experiments. A reference experiment was performed under the same conditions with the same volume of DMSO-d6 (Eurisotop) as used for the compound titration. Changes in the DNA structure were detected recording NMR Imino NOESY spectra at 10°C, using 100µM duplex-DNA, compound to a final concentration of 500 and 50µM ^{2}H(~100%), ^{15}N-labeled $RelA_{19\text{-}291}$ dimer in a 100mM deuterated d11-Tris-HCl buffer (pH 7.5, 75mM NaCl, 5mM d10-DTT and 10% D_2O) in different order.

Static light scattering (SLS). Static light scattering (SLS) experiments were performed at 30°C using a Viscotek TDA 305 triple array detector (Malvern Instruments) downstream to an Äkta Purifier (GE Healthcare) equipped with an analytical size exclusion column (Superdex 75 or 200 10/300 GL, GE Healthcare) at 277K. The samples were run in 50mM Tris-HCl pH 7.5, 150mM NaCl, 1mM EDTA and 5mM DTT with a concentration of 2mg/ml for the protein and a ratio of 1:2 protein:DNA at a flow rate of 0.5ml/min. The molecular masses of the samples were calculated from the refractive index and right-angle light-scattering signals using Omnisec (Malvern Instruments). The SLS detector was calibrated with a 4mg/ml BSA solution with 66.4kDa for the BSA monomer and a dn/dc value of 0.185ml/g for all protein samples.

Isothermal titration calorimetry. ITC measurements were carried out at 25 °C using a MicroCal PEAQ-ITC (Malvern Instruments Ltd). The titrations were performed in 50 mM HEPES pH 8.0, 100 mM NaCl and 1 mM mercaptoethanol and 1% DMSO. The

calorimetric titration consisted of 19 injections of 1.5µl of a 125µM DNA sample, into the reaction cell containing 400 µL of 25 µM RelA or to 25 µM RelA with 200 µM epirubicin/ aclarubicin, at a stirring speed of 1000 rpm. The heat of dilution was obtained by titrating DNA into the sample cell containing only buffer and this was subsequently subtracted from each experimental titration. For evaluating the effect of epirubicin bound to DNA on binding to RelA, a calorimetric titration consisted of 19 injections of 1.5 µL of a 125 µM DNA with 250 µM epirubicin mixture, into the reaction cell containing 400 µL of 25 µM RelA. For the determination of the binding affinity of the compounds to the DNA, a calorimetric titration was performed consisting of 19 injections of 1.5 µL of a 500 µM compound sample, into the reaction cell containing 400 µL of 50 µM DNA. The heat of dilution was obtained by titrating compound into the sample cell containing only buffer and this was subsequently subtracted from each experimental titration. For the determination of the binding affinity of the DNA to the protein, it was performed a calorimetric titration consisted of 19 injections of 1.5µL of a 125 µM DNA sample, into the reaction cell containing 400 µL of 25 µM RelA. The ITC data were analyzed using the MICROCAL PEAQ-ITC analysis software provided by Malvern.

Data availability

The relevant data supporting this study are available in Supplementary Information and provided by the authors upon request.

References

1. Medzhitov, R. & Horng, T. Transcriptional control of the inflammatory response. *Nature Reviews Immunology* (2009) doi:10.1038/nri2634.
2. Hayden, M. S. & Ghosh, S. Shared Principles in NF-κB Signaling. *Cell* (2008) doi:10.1016/j.cell.2008.01.020.
3. Chen, L. F. & Greene, W. C. Shaping the nuclear action of NF-κB. *Nature Reviews Molecular Cell Biology* (2004) doi:10.1038/nrm1368.
4. Baldwin, A. S. Series Introduction: The transcription factor NF-κB and human disease. *J. Clin. Invest.* (2001) doi:10.1172/jci11891.
5. Ghosh, S. & Baltimore, D. Activation in vitro of NF-κB" by phosphorylation of its inhibitor IκB". *Nature* (1990) doi:10.1038/344678a0.
6. Sun, S. C., Ganchi, P. A., Ballard, D. W. & Greene, W. C. NF-κB controls expression of inhibitor IκBα: Evidence for an inducible autoregulatory pathway. *Science (80-.).* (1993) doi:10.1126/science.8096091.
7. Beg, A. A. & Baldwin, A. S. The IκB proteins: Multifunctional regulators of Rel/NF-κB transcription factors. *Genes Dev.* (1993) doi:10.1101/gad.7.11.2064.
8. Huang, B., Yang, X. D., Lamb, A. & Chen, L. F. Posttranslational modifications of NF-κB: Another layer of regulation for NF-κB signaling pathway. *Cellular Signalling* (2010) doi:10.1016/j.cellsig.2010.03.017.
9. Hande, K. R. Clinical applications of anticancer drugs targeted to topoisomerase II. *Biochimica et Biophysica Acta - Gene Structure and Expression* (1998) doi:10.1016/S0167-4781(98)00134-1.
10. Tewey, K. M., Rowe, T. C., Yang, L., Halligan, B. D. & Liu, L. F. Adriamycin-induced DNA damage mediated by mammalian DNA topoisomerase II. *Science (80-.).* (1984) doi:10.1126/science.6093249.
11. Nitiss, J. L. Targeting DNA topoisomerase II in cancer chemotherapy. *Nature Reviews Cancer* (2009) doi:10.1038/nrc2607.
12. Eom, Y. W. *et al.* Two distinct modes of cell death induced by doxorubicin: Apoptosis and cell death through mitotic catastrophe accompanied by senescence-like phenotype. *Oncogene* (2005) doi:10.1038/sj.onc.1208627.
13. Pang, B. *et al.* Drug-induced histone eviction from open chromatin contributes to the chemotherapeutic effects of doxorubicin. *Nat. Commun.* (2013) doi:10.1038/ncomms2921.
14. Yang, F., Kemp, C. J. & Henikoff, S. Doxorubicin enhances nucleosome turnover

around promoters. *Curr. Biol.* (2013) doi:10.1016/j.cub.2013.03.043.

15. Figueiredo, N. *et al.* Anthracyclines induce DNA damage response-mediated protection against severe sepsis. *Immunity* (2013) doi:10.1016/j.immuni.2013.08.039.
16. Köse-Vogel, N. *et al.* Transcriptional Suppression of the NLRP3 Inflammasome and Cytokine Release in Primary Macrophages by Low-Dose Anthracyclines. *Cells* **9**, (2020).
17. Neves-Costa, A. & Moita, L. F. Modulation of inflammation and disease tolerance by DNA damage response pathways. *FEBS J.* **284**, (2017).
18. Millour, J. *et al.* ATM and p53 regulate FOXM1 expression via E2F in breast cancer epirubicin treatment and resistance. *Mol. Cancer Ther.* (2011) doi:10.1158/1535-7163.MCT-11-0024.
19. Maréchal, A. & Zou, L. DNA damage sensing by the ATM and ATR kinases. *Cold Spring Harb. Perspect. Biol.* (2013) doi:10.1101/cshperspect.a012716.
20. Piret, B., Schoonbroodt, S. & Piette, J. The ATM protein is required for sustained activation of NF-κB following DNA damage. *Oncogene* (1999) doi:10.1038/sj.onc.1202541.
21. Li, Y. *et al.* Expression of ATM in ataxia telangiectasia fibroblasts rescues defects in DNA double-strand break repair in nuclear extracts. *Environ. Mol. Mutagen.* (2001) doi:10.1002/em.1020.
22. Wu, Z. H., Shi, Y., Tibbetts, R. S. & Miyamoto, S. Molecular linkage between the kinase ATM and NF-κB signaling in response to genotoxic stimuli. *Science (80-.).* (2006) doi:10.1126/science.1121513.
23. Caporossi, D. *et al.* Hypersensitivity of lymphoblastoid lines derived from ataxia telangiectasia patients to the induction of chromosomal aberrations by etoposide (VP-16). *Mutat. Res. - Fundam. Mol. Mech. Mutagen.* (1993) doi:10.1016/0027-5107(93)90167-E.
24. Banáth, J. P. & Olive, P. L. Expression of phosphorylated histone H2AX as a surrogate of cell killing by drugs that create DNA double-strand breaks. *Cancer Res.* (2003).
25. Chang, J. T. & Nevins, J. R. GATHER: A systems approach to interpreting genomic signatures. *Bioinformatics* (2006) doi:10.1093/bioinformatics/btl483.
26. Campbell, K. J., Rocha, S. & Perkins, N. D. Active repression of antiapoptotic gene expression by RelA(p65) NF-κB. *Mol. Cell* (2004) doi:10.1016/S1097-

2765(04)00131-5.

27. Ho, W. C., Dickson, K. M. & Barker, P. A. Nuclear factor-κB induced by doxorubicin is deficient in phosphorylation and acetylation and represses nuclear factor-κB-dependent transcription in cancer cells. *Cancer Res.* (2005) doi:10.1158/0008-5472.CAN-04-3494.

28. Wang, C. Y., Mayo, M. W. & Baldwin, A. S. TNF- and cancer therapy-induced apoptosis: Potentiation by inhibition of NF-κB. *Science (80-.).* (1996) doi:10.1126/science.274.5288.784.

29. Hochrainer, K., Racchumi, G. & Anrather, J. Hypo-phosphorylation leads to nuclear retention of NF-κB p65 due to impaired IκBα gene synthesis. *FEBS Lett.* (2007) doi:10.1016/j.febslet.2007.10.056.

30. Liu, J., Zheng, H., Tang, M., Ryu, Y. C. & Wang, X. A therapeutic dose of doxorubicin activates ubiquitin-proteasome system-mediated proteolysis by acting on both the ubiquitination apparatus and proteasome. *Am. J. Physiol. - Hear. Circ. Physiol.* (2008) doi:10.1152/ajpheart.01052.2008.

31. Tanaka, T., Yamaguchis, J., Shojis, K. & Nangakus, M. Anthracycline inhibits recruitment of hypoxia-inducible transcription factors and suppresses tumor cell migration and cardiac angiogenic response in the host. *J. Biol. Chem.* (2012) doi:10.1074/jbc.M112.374587.

32. Toledano, M. B., Ghosh, D., Trinh, F. & Leonard, W. J. N-terminal DNA-binding domains contribute to differential DNA-binding specificities of NF-kappa B p50 and p65. *Mol. Cell. Biol.* (1993) doi:10.1128/mcb.13.2.852.

33. Anrather, J., Csizmadia, V., Soares, M. P. & Winkler, H. Regulation of NF-κB RelA phosphorylation and transcriptional activity by p21(ras) and protein kinase Cζ in primary endothelial cells. *J. Biol. Chem.* (1999) doi:10.1074/jbc.274.19.13594.

34. Mulero, M. C. *et al.* DNA-binding affinity and transcriptional activity of the RelA homodimer of nuclear factor κb are not correlated. *J. Biol. Chem.* (2017) doi:10.1074/jbc.M117.813980.

35. Chen, Y. Q., Ghosh, S. & Ghosh, G. A novel DNA recognition mode by the NF-κb p65 homodimer. *Nat. Struct. Biol.* (1998) doi:10.1038/nsb0198-67.

36. Furusawa, H., Nakayama, H., Funasaki, M. & Okahata, Y. Kinetic characterization of small DNA-binding molecules interacting with a DNA strand on a quartz crystal microbalance. *Anal. Biochem.* (2016)

doi:10.1016/j.ab.2015.09.015.

37. Utsuno, K. & Tsuboi, M. Degree of DNA unwinding caused by the binding of aclacinomycin A. *Chem. Pharm. Bull.* (1997) doi:10.1248/cpb.45.1551.
38. Skovsgaard, T. Pharmacodynamic aspects of aclarubicin with special reference to daunorubicin and doxorubicin. *Eur. J. Haematol.* (1987) doi:10.1111/j.1600-0609.1987.tb00018.x.
39. Katenkamp, U., Stutter, E., Petri, I., Gollmick, F. A. & Berg, H. Interaction of anthracycline antibiotics with biopolymers VIII. binding parameters of aclacinomycin A to Dna. *J. Antibiot. (Tokyo).* (1983) doi:10.7164/antibiotics.36.1222.
40. Temperini, C. *et al.* The crystal structure of the complex between a disaccharide anthracycline and the DNA hexamer d(CGATCG) reveals two different binding sites involving two DNA duplexes. *Nucleic Acids Research* (2003) doi:10.1093/nar/gkg245.
41. Chaires, J. B. A small molecule - DNA binding landscape. *Biopolymers* (2015) doi:10.1002/bip.22660.
42. Frederick, C. A. *et al.* Structural Comparison of Anticancer Drug-DNA Complexes: Adriamycin and Daunomycin. *Biochemistry* (1990) doi:10.1021/bi00462a016.
43. Chen, Y. Q., Sengchanthalangsy, L. L., Hackett, A. & Ghosh, G. NF-κB p65 (RelA) homodimer uses distinct mechanisms to recognize DNA targets. *Structure* (2000) doi:10.1016/S0969-2126(00)00123-4.
44. Bergqvist, S. *et al.* Kinetic enhancement of NF-κB·DNA dissociation by IκBα. *Proc. Natl. Acad. Sci. U. S. A.* (2009) doi:10.1073/pnas.0908797106.
45. Zunino, F., Pratesi, G. & Perego, P. Role of the sugar moiety in the pharmacological activity of anthracyclines: Development of a novel series of disaccharide analogs. *Biochem. Pharmacol.* (2001) doi:10.1016/S0006-2952(01)00522-6.
46. Arlt, A. *et al.* Inhibition of NF-κB sensitizes human pancreatic carcinoma cells to apoptosis induced by etoposide (VP16) or doxorubicin. *Oncogene* (2001) doi:10.1038/sj.onc.1204168.
47. Janssens, S., Tinel, A., Lippens, S. & Tschopp, J. PIDD Mediates NF-κB activation in response to DNA damage. *Cell* (2005) doi:10.1016/j.cell.2005.09.036.

48. Moura-alves, P. *et al.* An shRNA-Based Screen of Splicing Regulators Identifies SFRS3 as a Negative Regulator of IL-1b Secretion. **6**, 1–10 (2011).

49. Ewels, P., Magnusson, M., Lundin, S. & Käller, M. MultiQC: Summarize analysis results for multiple tools and samples in a single report. *Bioinformatics* (2016) doi:10.1093/bioinformatics/btw354.

50. Dobin, A. *et al.* STAR: Ultrafast universal RNA-seq aligner. *Bioinformatics* (2013) doi:10.1093/bioinformatics/bts635.

51. Love, M. I., Huber, W. & Anders, S. Moderated estimation of fold change and dispersion for RNA-seq data with DESeq2. *Genome Biol.* (2014) doi:10.1186/s13059-014-0550-8.

52. Stephens, M. False discovery rates: A new deal. *Biostatistics* (2017) doi:10.1093/biostatistics/kxw041.

53. De Almeida, S. F. *et al.* Splicing enhances recruitment of methyltransferase HYPB/Setd2 and methylation of histone H3 Lys36. *Nat. Struct. Mol. Biol.* (2011) doi:10.1038/nsmb.2123.

Figure 1

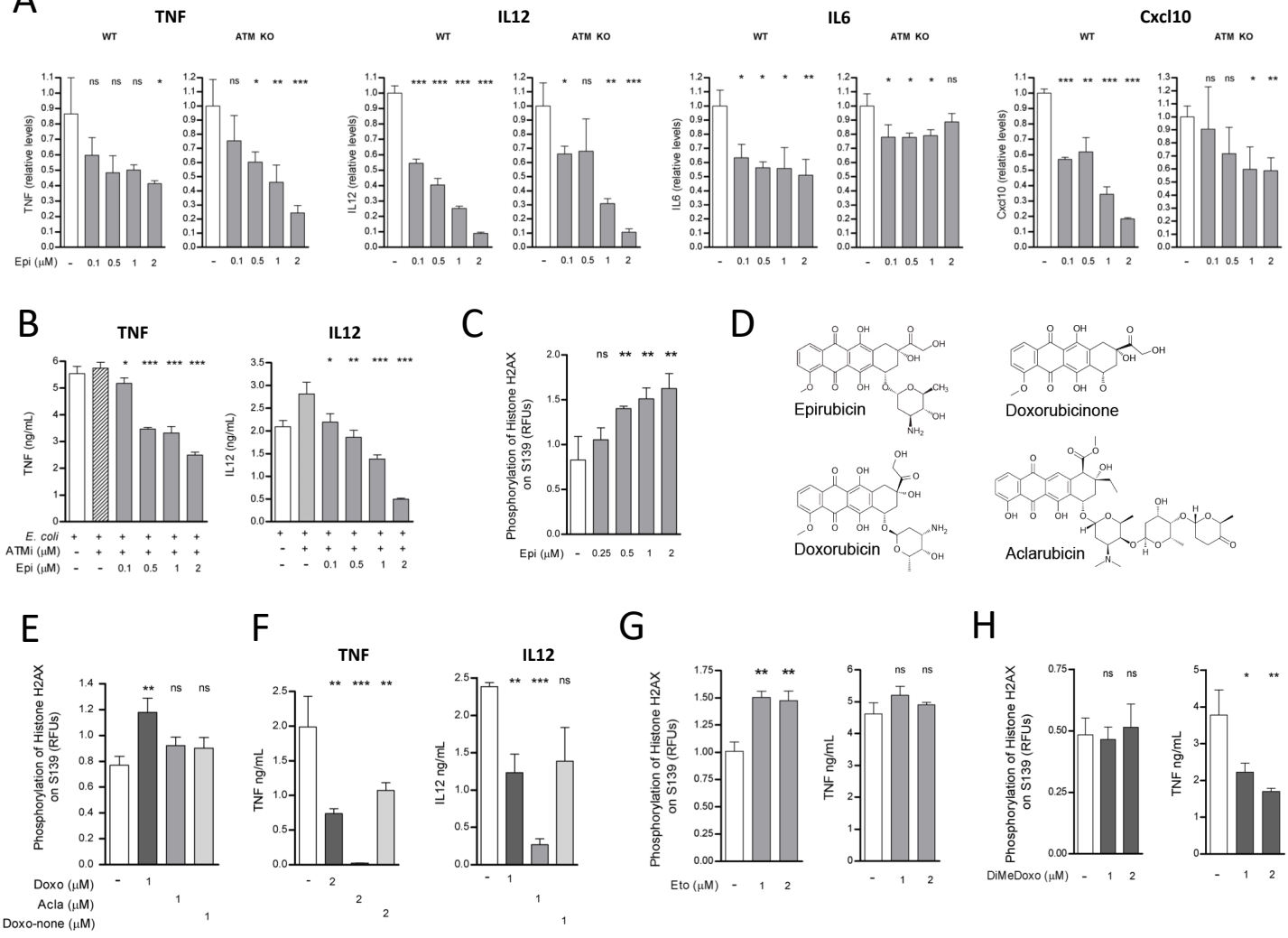
A
TNF
IL12
IL6
Cxcl10
WT
ATM KO
TNF (relative levels)
IL12 (relative levels)
IL6 (relative levels)
Cxcl10 (relative levels)
Epi (μM)
B
TNF
IL12
TNF (ng/mL)
IL12 (ng/mL)
E. coli
ATMi (μM)
Epi (μM)
C
Phosphorylation of Histone H2AX on S139 (RFUs)
Epi (μM)
D
Epirubicin
Doxorubicinone
Doxorubicin
Aclarubicin
E
Phosphorylation of Histone H2AX on S139 (RFUs)
Doxo (μM)
Acla (μM)
Doxo-none (μM)
F
TNF
IL12
TNF ng/mL
IL12 ng/mL
G
Phosphorylation of Histone H2AX on S139 (RFUs)
TNF ng/mL
Eto (μM)
H
Phosphorylation of Histone H2AX on S139 (RFUs)
TNF ng/mL
DiMeDoxo (μM)

Figure 2

A

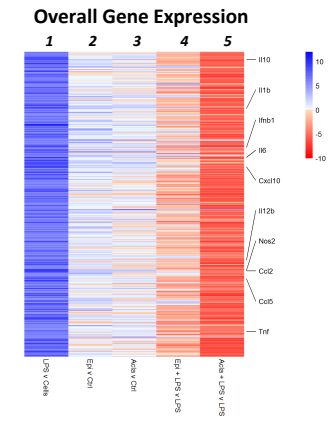

B

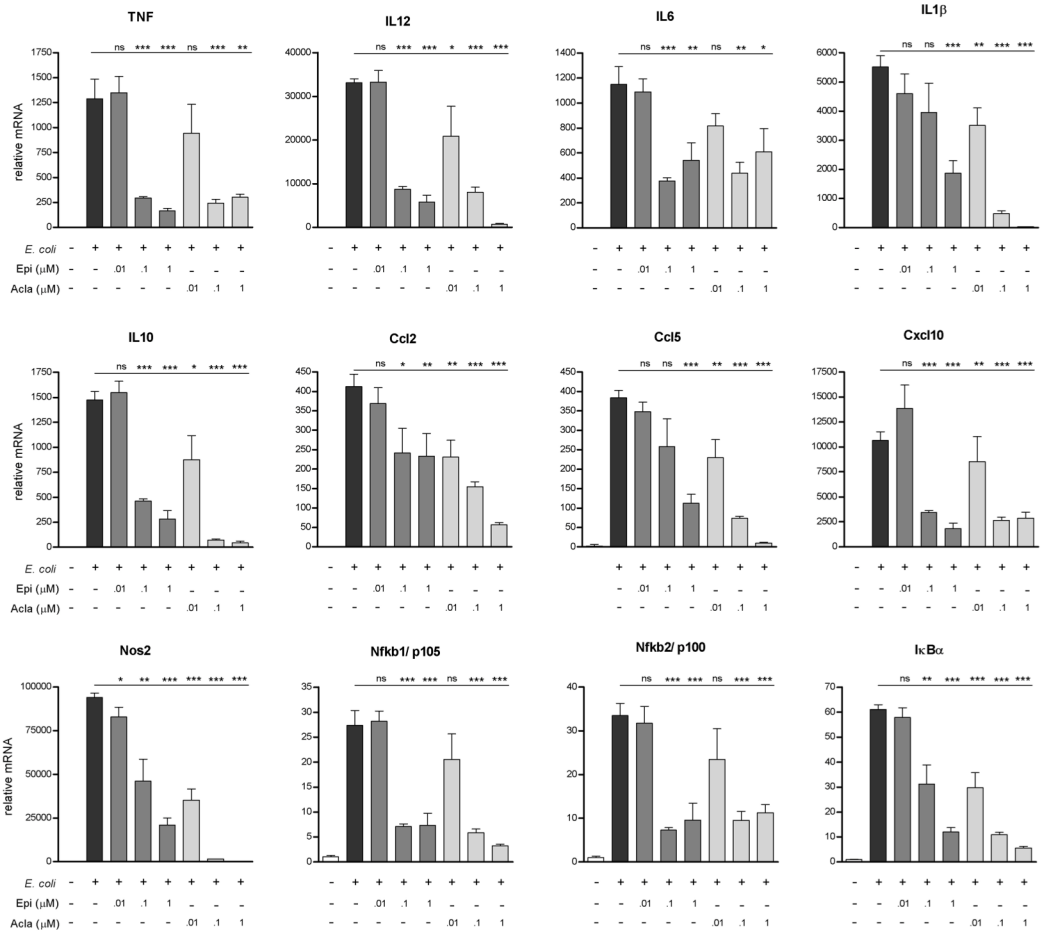

C

Molecular Signatures	Bayes factor
Interferon-stimulated response element (STAT1 & STAT2)	11,10
interferon regulatory factor 1 (IRF1)	5,23
Interferon regulatory factor 7 (IRF7)	4,73
Interferon regulatory factor 8 (IRF8)	4,64
NFKB RelA (p65)	4,10
Interferon regulatory factor 1 (IRF1)	3,18
NF-kappaB	2,63

D

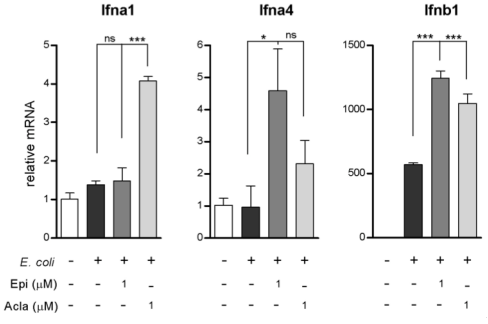

E

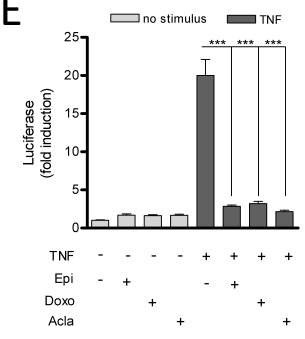

F

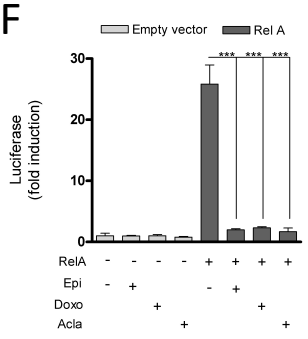

Figure 3

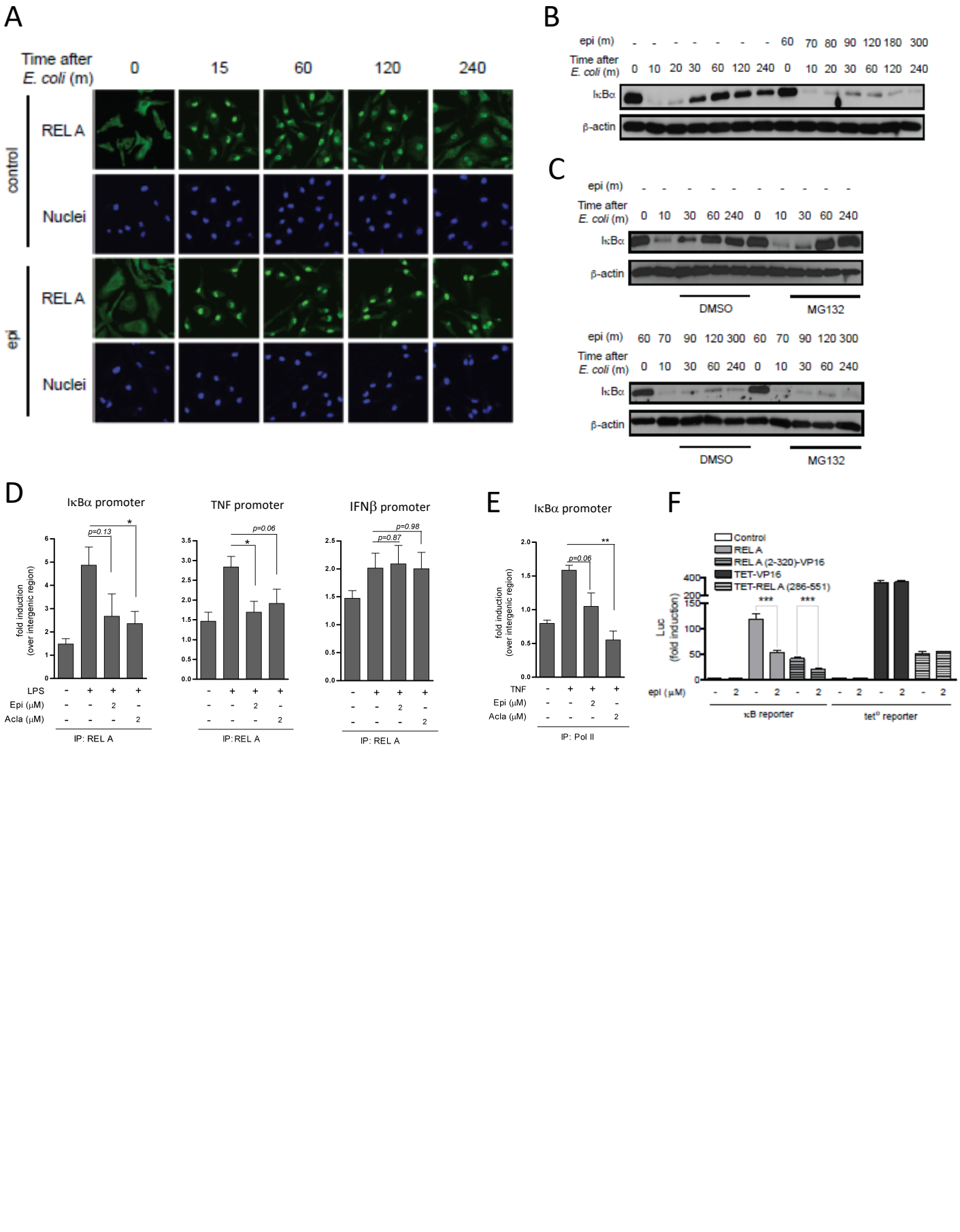
A
Time after E. coli (m)
0
15
60
120
240
control
REL A
Nuclei
epi
REL A
Nuclei
B
epi (m)
60 70 80 90 120 180 300
Time after E. coli (m)
0 10 20 30 60 120 240 0 10 20 30 60 120 240
IκBα
β-actin
C
epi (m)
Time after E. coli (m)
0 10 30 60 240 0 10 30 60 240
IκBα
β-actin
DMSO
MG132
epi (m)
60 70 90 120 300 60 70 90 120 300
Time after E. coli (m)
0 10 30 60 240 0 10 30 60 240
IκBα
β-actin
DMSO
MG132
D
IκBα promoter
TNF promoter
IFNβ promoter
fold induction (over intergenic region)
p=0.13
p=0.06
p=0.98
p=0.87
LPS
Epi (μM)
Acla (μM)
IP: REL A
IP: REL A
IP: REL A
E
IκBα promoter
p=0.06
fold induction (over intergenic region)
TNF
Epi (μM)
Acla (μM)
IP: Pol II
F
Control
REL A
REL A (2-320)-VP16
TET-VP16
TET-REL A (286-551)
Luc (fold induction)
epi (μM)
κB reporter
tetO reporter

Figure 4

A

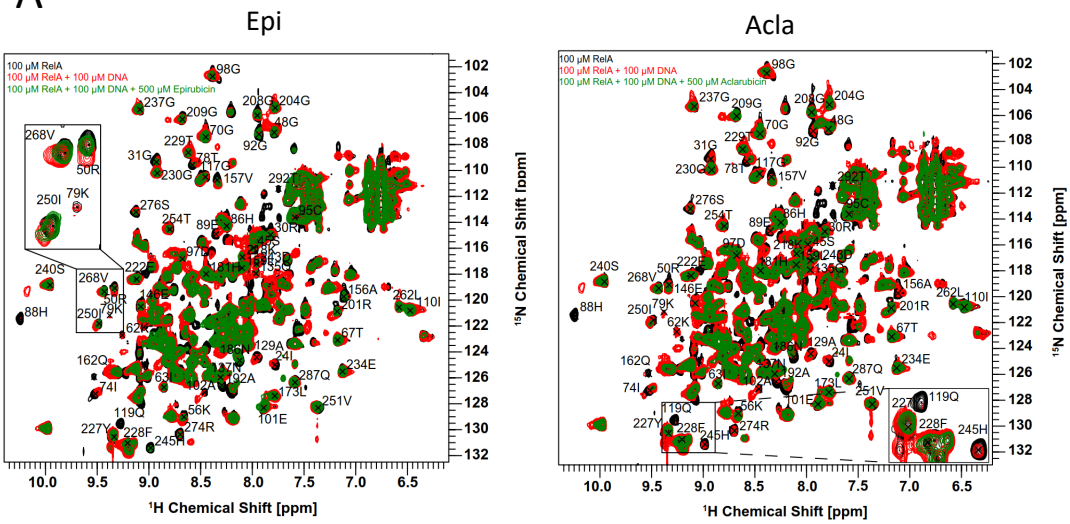
Epi
Acla
100 μM RelA
100 μM RelA + 100 μM DNA
100 μM RelA + 100 μM DNA + 500 μM Epirubicin
100 μM RelA + 100 μM DNA + 500 μM Aclarubicin
^{15}N Chemical Shift [ppm]
^{1}H Chemical Shift [ppm]

B

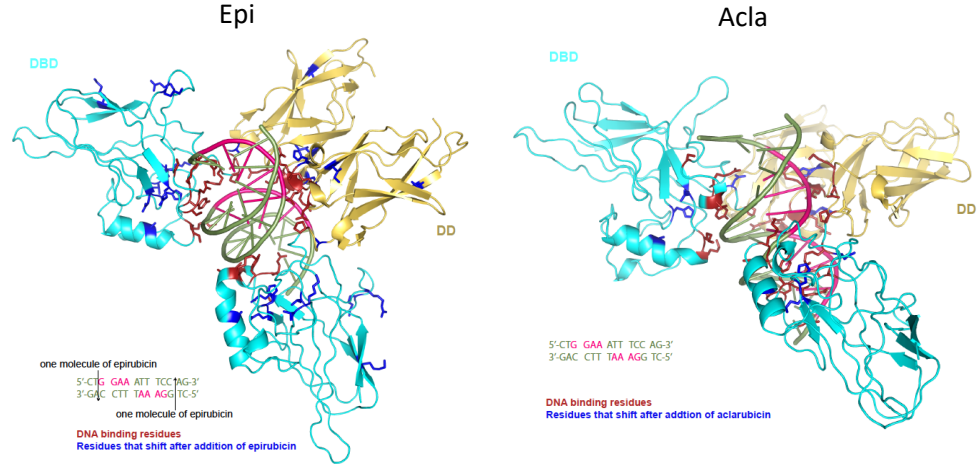
Epi
Acla
DBD
DD
one molecule of epirubicin
5′-CTG GAA ATT TCC AG-3′
3′-GAC CTT TAA AGG TC-5′
DNA binding residues
Residues that shift after addition of epirubicin
Residues that shift after addtion of aclarubicin

Table 1

Syringe	Cell	K_D (μM)	ΔH (kJ/mol)	-TΔS (kJ/mol)
500 μM Epirubicin	25 μM DNA	11.4 ± 2.3	-14.10 ± 2.16	-14.1
500 μM Aclarubicin	25 μM DNA	7.30 ± 1.4	-35.70 ± 1.70	6.8
125 μM DNA	25 μM p65	0.69 ± 0.17	-64.90 ± 4.81	-100
125 μM DNA	25 μM p65 +200 μM Epirubicin	1.01 ± 0.02	-307 ± 14.5	272
125 μM DNA	25 μM p65 + 200 μM Aclarubicin	0.74 ± 0.32	-335 ± 39.5	300
125 μM DNA +250 μM Epirubicin	25 μM P65	5.00 ± 0.23	-53.8 ± 4.07	54.1
500 μM Epirubicin	50 μM p65	Weak		
500 μM Aclarubicin	50 μM p65	Weak		

Supp Figure 1

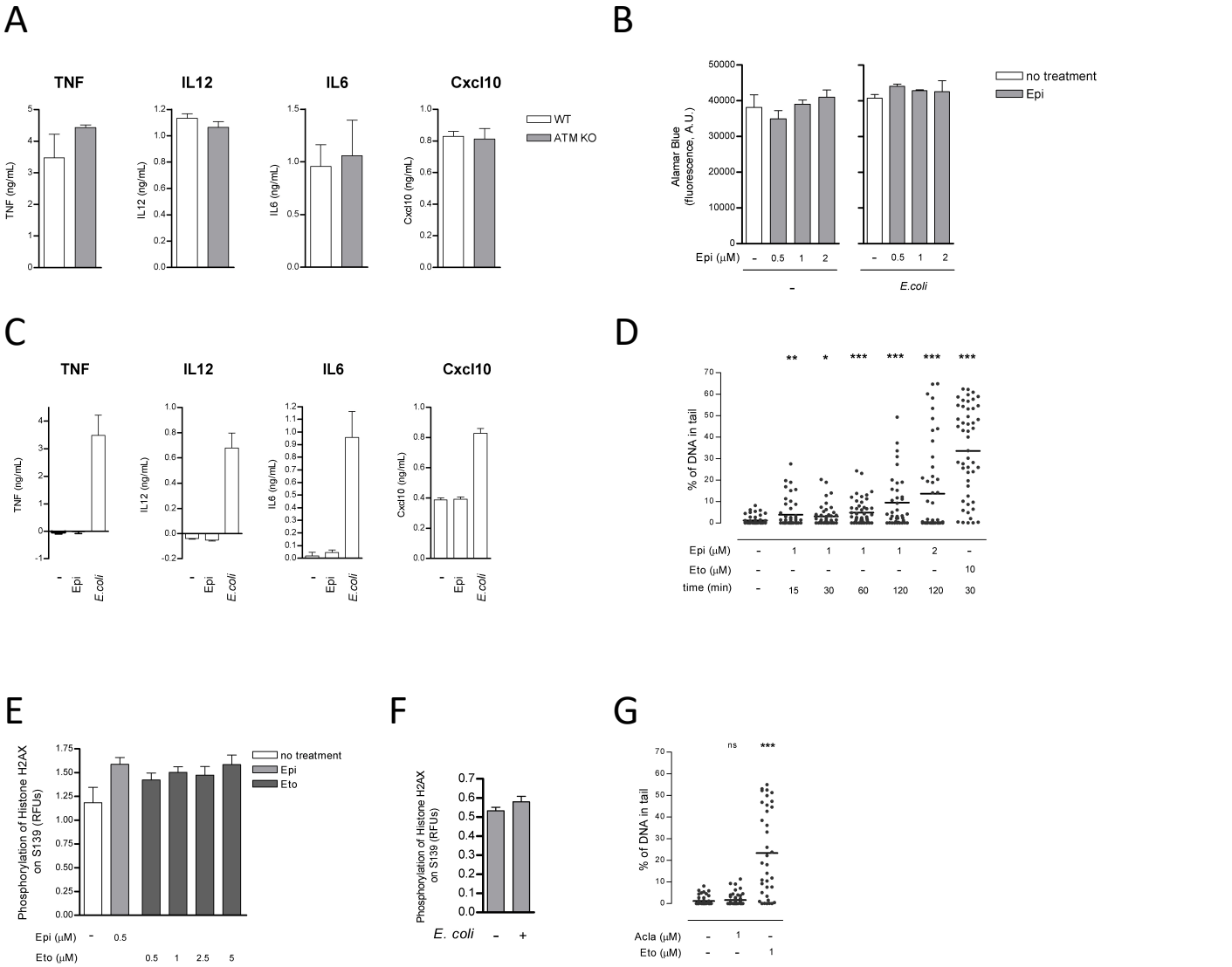

Supp Figure 2

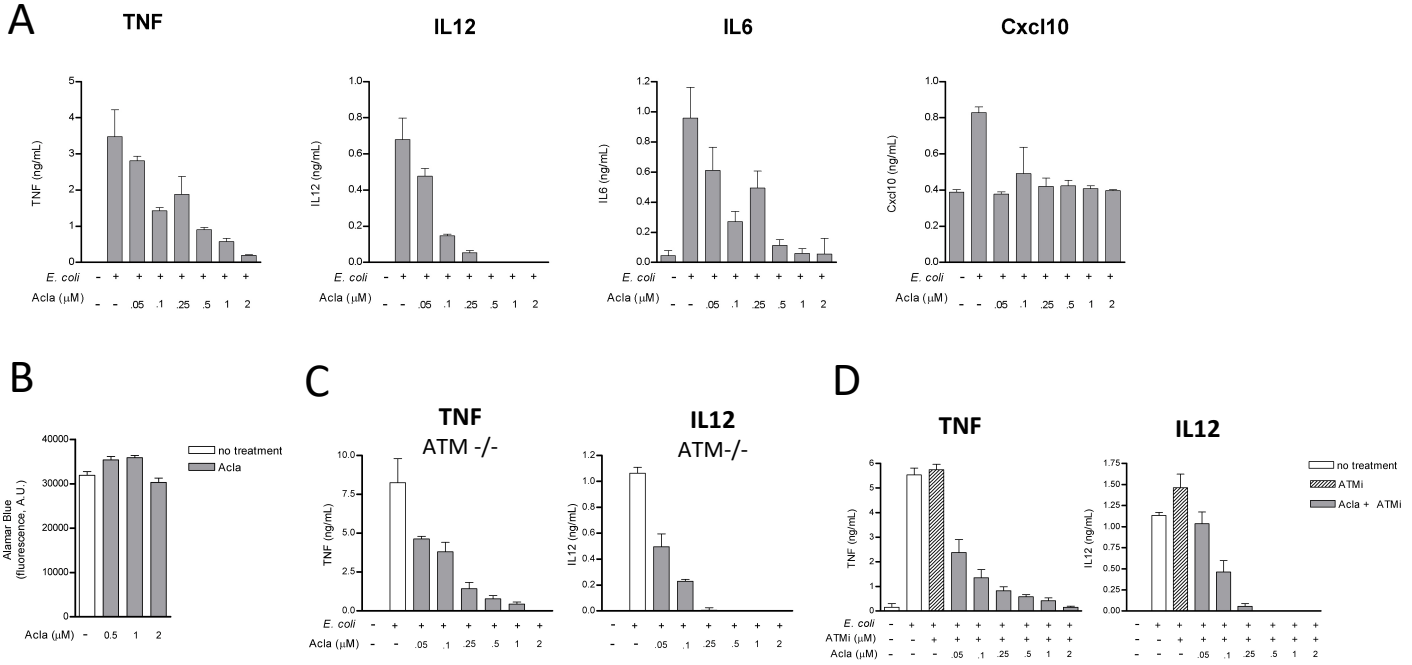

Supp Figure 3

A

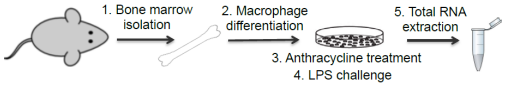

B

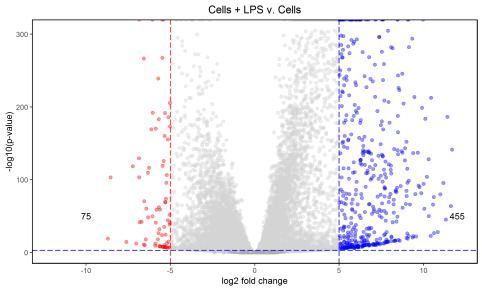

C

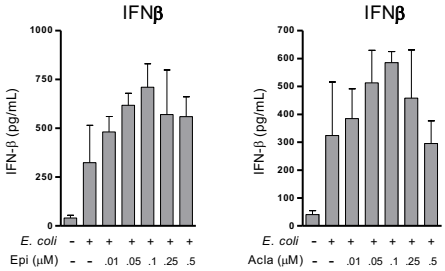

D

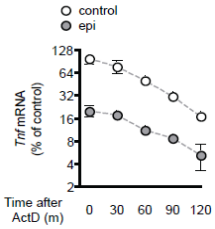

E

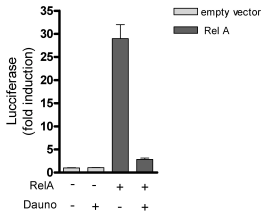

F

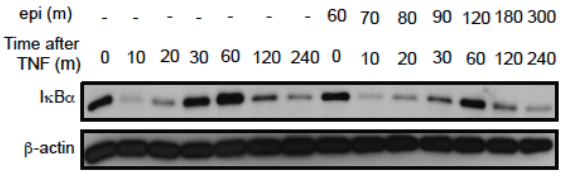

Supp Table 1 DAVID functional analysis

Epi

Cluster Enrichment Score: 7.128357433869625	
Category	**Term**
UniProt Keywords	Inflammatory response
UniProt Keywords	Immunity
UniProt Keywords	Innate immunity
GO Biological Process	Immune system process
GO Biological Process	innate immune response

Cluster Enrichment Score: 6.570030482177336	
Category	**Term**
KEGG PATHWAY	Cytokine-cytokine receptor interaction
GO Biological Process	Immune response
UniProt Keywords	Cytokine
GO Biological Process	Cytokine activity

Cluster Enrichment Score: 1.944662280964713	
Category	**Term**
INTERPRO	Tumour necrosis factor
SMART	TNF
INTERPRO	Tumour necrosis factor, conserved site
INTERPRO	Tumour necrosis factor alpha/beta/c
Go Molecular Function	Tumor necrosis factor receptor binding
INTERPRO	Tumour necrosis factor-like domain

Acla

Cluster Enrichment Score: 26.374073343937372	
Category	**Term**
UniProt Keywords	Immunity
GO Biological Process	Immune system process
UniProt Keywords	Innate immunity
GO Biological Process	Innate immune response

Cluster Enrichment Score: 9.853989037368624	
Category	**Term**
GO Biological Process	Immune response
KEGG PATHWAY	Cytokine-cytokine receptor interaction
UniProt Keywords	Cytokine
Go Molecular Function	Cytokine activity

Cluster Enrichment Score: 3.8322404478340935	
Category	**Term**
GO Biological Process	Cellular response to interferon-gamma
GO Biological Process	Cell chemotaxis
GO Biological Process	Chemotaxis
UniProt Keywords	Chemotaxis
GO Biological Process	Chemokine-mediated signaling pathway
INTERPRO	CC chemokine, conserved site
INTERPRO	Chemokine interleukin-8-like domain
GO Biological Process	Neutrophil chemotaxis
Go Molecular Function	Chemokine activity
SMART	SCY
GO Biological Process	Lymphocyte chemotaxis
GO Biological Process	Monocyte chemotaxis
GO Biological Process	Positive regulation of natural killer cell chemotaxis
Go Molecular Function	CCR chemokine receptor binding
GO Biological Process	Macrophage chemotaxis
GO Biological Process	Eosinophil chemotaxis

Supp Figure 4

A

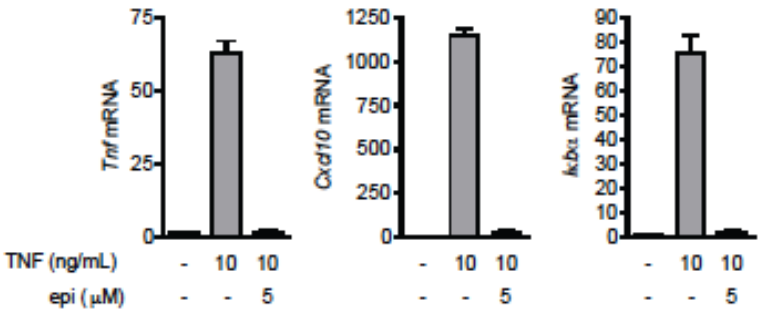

B

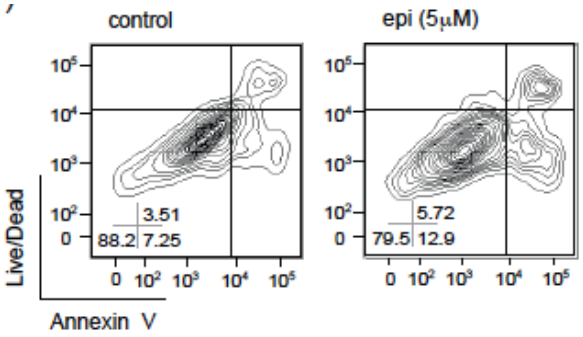

C

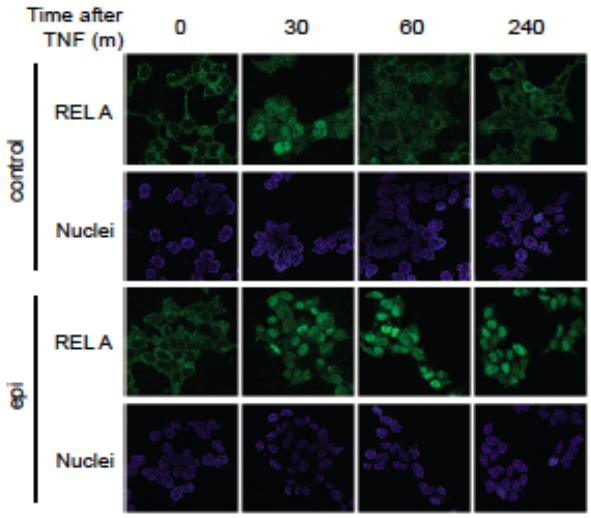

D

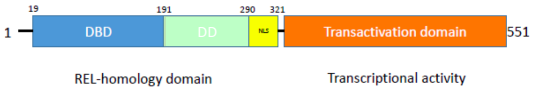

Supp Figure 5

A

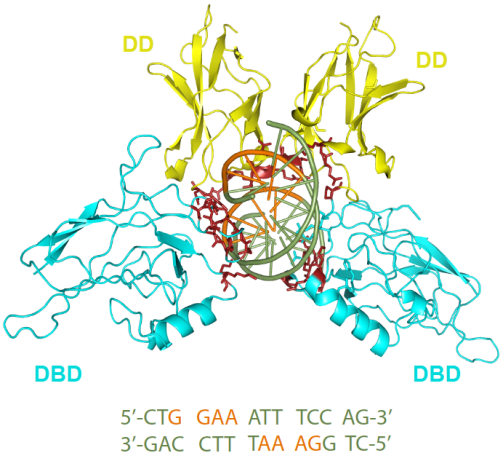

B

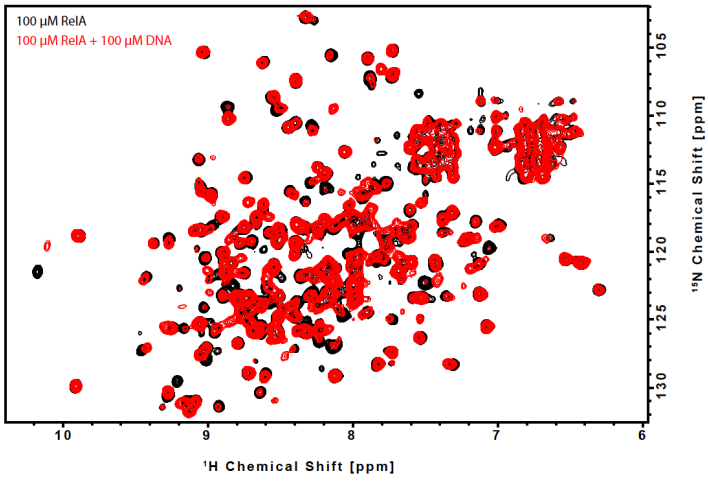

Supp Figure 6

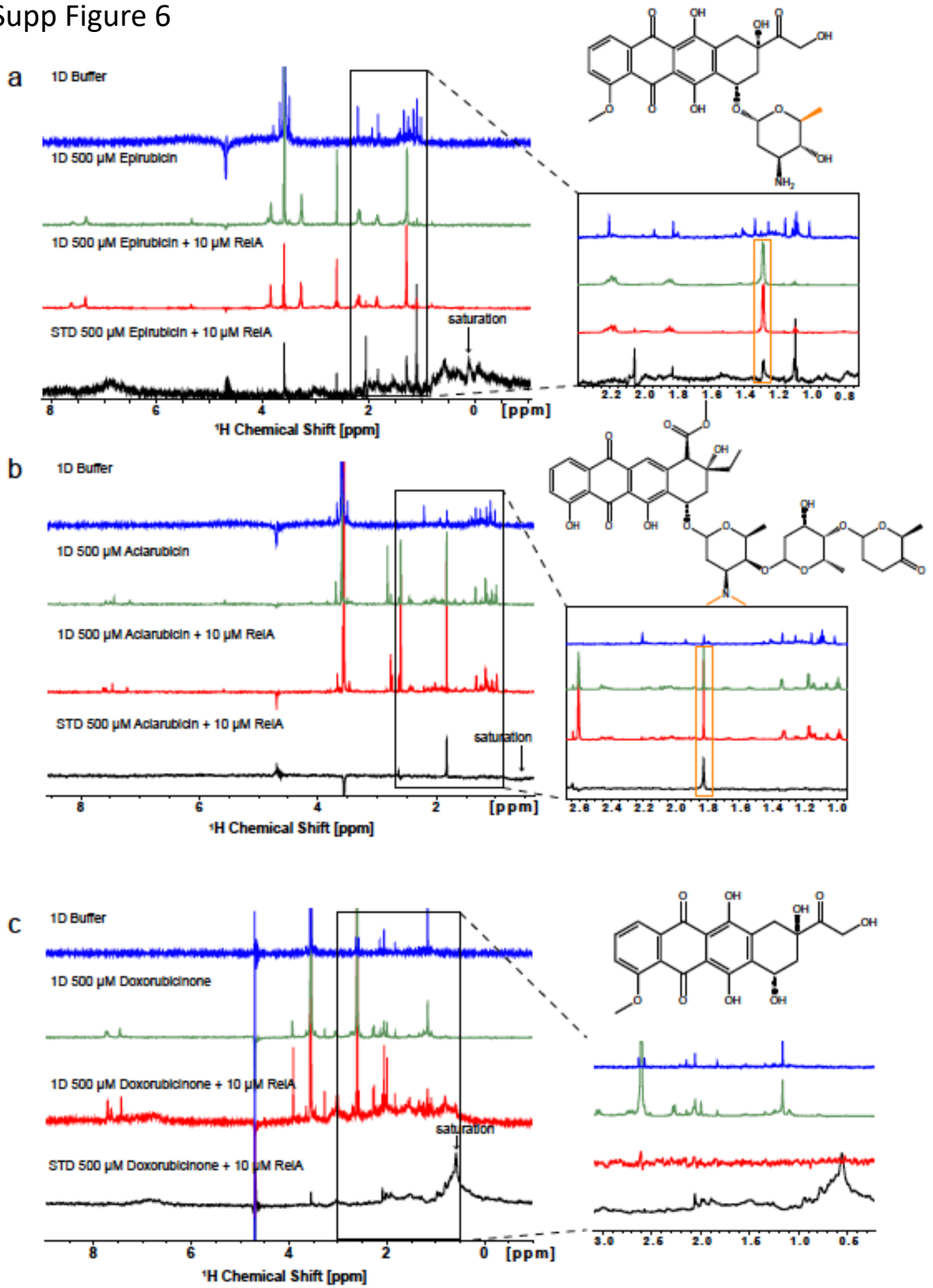

Supp Figure 7

Epi

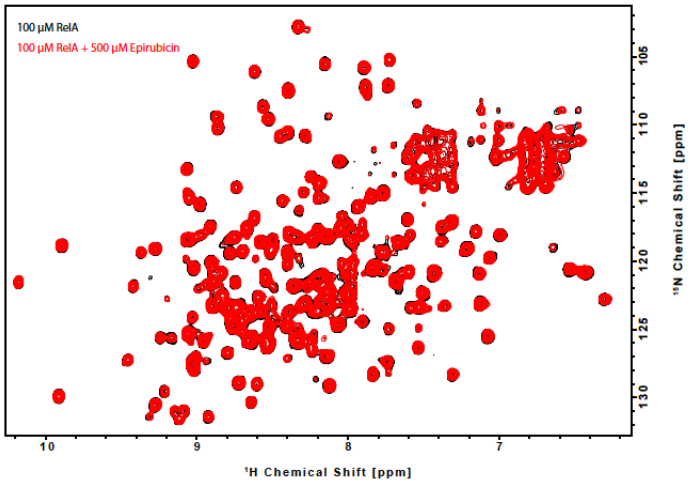

b

Acla

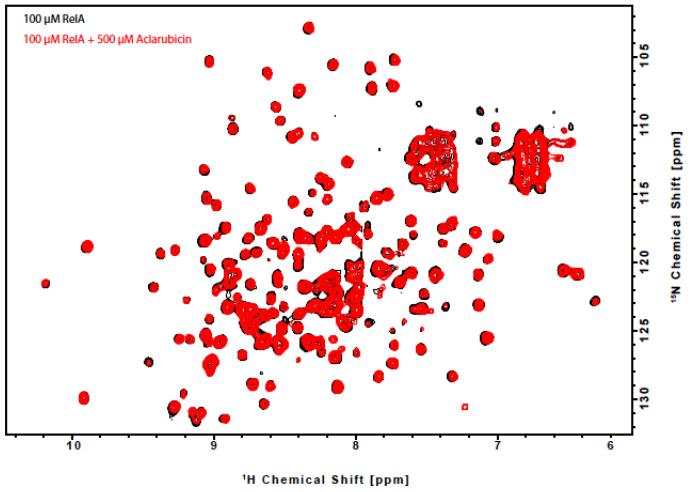

Supp Figure 8

Epi

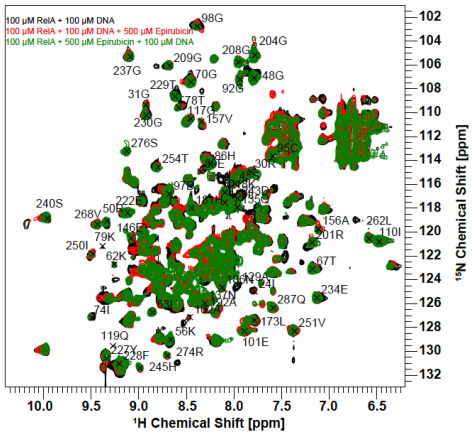

Acla